Genetics: Early Online, published on March 21, 2017 as 10.1534/genetics.116.198820

The NCA-1 and NCA-2 ion channels function downstream of G_q and Rho to regulate locomotion in *C. elegans*

Irini Topalidou[*], Pin-An Chen[†], Kirsten Cooper[*,1], Shigeki Watanabe[†,2], Erik M. Jorgensen[†], Michael Ailion[*]

[*]Department of Biochemistry, University of Washington, Seattle, WA 98195

[†]Howard Hughes Medical Institute, Department of Biology, University of Utah, Salt Lake City, UT 84112

[1]Current Address: Fred Hutchinson Cancer Research Center, Seattle, WA 98109

[2]Current Address: Department of Cell Biology, Johns Hopkins University, Baltimore, MD 21205

Copyright 2017.

Running Title: Gq signaling activates NCA channels through Rho

key words: G_q signaling, Rho small GTPase, NCA/NALCN ion channels, *C. elegans*, G protein

Corresponding author:

Michael Ailion

Department of Biochemistry

University of Washington

Box 357350

1705 NE Pacific St

Seattle, WA 98195

Phone: 206-685-0111

email: mailion@uw.edu

Abstract

The heterotrimeric G protein G_q positively regulates neuronal activity and synaptic transmission. Previously, the Rho guanine nucleotide exchange factor Trio was identified as a direct effector of G_q that acts in parallel to the canonical G_q effector phospholipase C. Here we examine how Trio and Rho act to stimulate neuronal activity downstream of G_q in the nematode *Caenorhabditis elegans*. Through two forward genetic screens, we identify the cation channels NCA-1 and NCA-2, orthologs of mammalian NALCN, as downstream targets of the G_q/Rho pathway. By performing genetic epistasis analysis using dominant activating mutations and recessive loss-of-function mutations in the members of this pathway, we show that NCA-1 and NCA-2 act downstream of G_q in a linear pathway. Through cell-specific rescue experiments, we show that function of these channels in head acetylcholine neurons is sufficient for normal locomotion in *C. elegans*. Our results suggest that NCA-1 and NCA-2 are physiologically relevant targets of neuronal G_q-Rho signaling in *C. elegans*.

Introduction

Heterotrimeric G proteins play central roles in altering neuronal activity and synaptic transmission in response to experience or changes in the environment. G_q is one of the four types of heterotrimeric G protein alpha subunits in animals (Wilkie *et al.* 1992). G_q is widely expressed in the mammalian brain (Wilkie *et al.* 1991) where it acts to stimulate neuronal activity (Krause *et al.* 2002; Gamper *et al.* 2004; Coulon *et al.* 2010). Unlike mammals which have four members of the G_q family, *C. elegans* has only a single $G_q\alpha$ gene *egl-30* (Brundage *et al.* 1996). Loss-of-function and gain-of-function mutants in *egl-30* are viable but have strong neuronal phenotypes, affecting locomotion, egg-laying, and sensory behaviors (Brundage *et al.* 1996; Lackner *et al.* 1999; Bastiani *et al.* 2003; Matsuki *et al.* 2006; Esposito *et al.* 2010; Adachi *et al.* 2010). We aim to identify the downstream pathways by which G_q signaling alters neuronal activity.

In the canonical G_q pathway, G_q activates phospholipase Cβ (PLC) to cleave the lipid phosphatidylinositol 4,5,-bisphosphate (PIP2) into the second messengers diacylglycerol (DAG) and inositol trisphosphate (IP3). This pathway operates in both worms and mammals, but in both systems, a number of PLC-independent effects of G_q have been described (Lackner *et al.* 1999; Miller *et al.* 1999; Vogt *et al.* 2003; Bastiani *et al.* 2003; Sánchez-Fernández *et al.* 2014). Using a genetic screen for suppressors of activated G_q, we identified the Rho guanine nucleotide exchange factor (GEF) Trio as a direct effector of G_q in a second major conserved G_q signal transduction pathway independent of the PLC pathway (Williams *et al.* 2007). Biochemical and structural studies demonstrated that G_q directly binds and activates RhoGEF proteins in both worms and mammals (Lutz *et al.* 2005, 2007; Williams *et al.* 2007).

Trio acts as a RhoGEF for the small G protein Rho, a major cellular switch that affects a number of cellular processes ranging from regulation of the cytoskeleton to transcription (Etienne-Manneville and Hall 2002; Jaffe and Hall 2005). In *C. elegans* neurons, Rho regulates synaptic transmission downstream of the G_{12}-class G protein GPA-12 via at least two pathways, one

dependent on the diacylglycerol kinase DGK-1 and one independent of DGK-1 (McMullan *et al.* 2006; Hiley *et al.* 2006). Here we investigate what targets act downstream of Rho in the G_q signaling pathway to regulate neuronal activity. Through two forward genetic screens, we identify the cation channels NCA-1 and NCA-2 (NALCN in mammals) as downstream targets of the G_q-Rho pathway. The NALCN channel is a relative of voltage-gated cation channels that has been suggested to be a sodium leak channel required for the propagation of neuronal excitation and the fidelity of synaptic transmission (Lu *et al.* 2007; Jospin *et al.* 2007; Yeh *et al.* 2008). However, there is controversy over whether NALCN is indeed a sodium leak channel (Senatore *et al.* 2013; Senatore and Spafford 2013; Boone *et al.* 2014). It is also unclear how NALCN is gated and what pathways activate the channel. Two studies have shown that NALCN-dependent currents can be activated by G protein-coupled receptors, albeit independently of G proteins (Lu *et al.* 2009; Swayne *et al.* 2009), and another study showed that the NALCN leak current can be activated by low extracellular calcium via a G protein-dependent pathway (Lu *et al.* 2010). Our data here suggest that the worm NALCN orthologs NCA-1 and NCA-2 are activated by Rho acting downstream of G_q in a linear pathway.

Materials and Methods

Strains

Worm strains were cultured using standard methods (Brenner, 1974). A complete list of strains and mutations is provided in the strain list (Table S1).

Isolation of suppressors of activated G_q

We performed an ENU mutagenesis to screen for suppressors of the hyperactive locomotion of an activated G_q mutant, *egl-30(tg26)* (Ailion *et al.* 2014). From approximately 47,000 mutagenized haploid genomes, we isolated 10 mutants that had a fainter phenotype when outcrossed away from the *egl-30(tg26)* mutation. By mapping and complementation testing, we assigned these ten mutants to three genes: three *unc-79* mutants (*yak37*, *yak61*, and *yak73*), six *unc-80* mutants (*ox329*, *ox330*, *yak8*, *yak35*, *yak36*, and *yak56*), and one *nlf-1* mutant (*ox327*). Complementation tests of *ox329* and *ox330* were performed by crossing heterozygous mutant males to *unc-79(e1068)* and *unc-13(n2813) unc-80(ox301)* hermaphrodites. Complementation tests of *yak* alleles were performed by crossing heterozygous mutant males (*m/+*) to *unc-79(e1068)* and *unc-80(ox330)* mutant hermaphrodites. We assessed the fainting phenotype of at least five male or hermaphrodite cross-progeny by touching animals on the head and scoring whether animals fainted within five seconds. Control crosses with wild-type males demonstrated that *unc-79/+* and *unc-80/+* heterozygous males and hermaphrodites are phenotypically wild-type, demonstrating that these mutants are fully recessive.

Isolation of suppressors of activated G_o

We first isolated suppressors of the activated G_o mutant *unc-109(n499)* by building double mutants of *unc-109(n499)* with the activated G_q allele *egl-30(tg26)*. Unlike *unc-109(n499)*

homozygotes which are lethal, *egl-30(tg26) unc-109(n499)* homozygotes are viable, but paralyzed and sterile, indicating that activated G_q partially suppresses activated G_o. We built a balanced heterozygote strain *egl-30(tg26) unc-109(n499)/egl-30(tg26) unc-13(e51) gld-1(q126)* in which the worms move infrequently and slowly. We mutagenized these heterozygous animals with ENU and screened for F1 progeny that moved better. From a screen of approximately 16,000 mutagenized haploid genomes, we isolated two apparent *unc-109* intragenic mutants, *ox303* and *ox304*. *ox303* is a strong *unc-109* loss-of-function allele, as evidenced by the fact that *egl-30(tg26) unc-109(n499 ox303)/egl-30(tg26) unc-13(e51) gld-1(q126)* mutants resembled *egl-30(tg26)* mutants (i.e. hyperactive). Additionally, *unc-109(n499 ox303)* mutants are hyperactive. *ox304*, however, appears to be a partial loss-of-function mutant, because the *egl-30(tg26) unc-109(n499 ox304)/egl-30(tg26) unc-13(e51) gld-1(q126)* mutant is not hyperactive like the *egl-30(tg26)* strain. Also, *unc-109(n499 ox304)* homozygote animals are viable, show very little spontaneous movement, and have a straight posture. However, when stimulated by transfer to a new plate they are capable of coordinated movements. This strain was used for mapping and sequencing experiments that demonstrated that *unc-109* is allelic to *goa-1*, encoding the worm G_o ortholog (see below). The *unc-109(n499 ox304)* strain was also used as the starting point for a second screen to isolate extragenic suppressors of activated G_o.

Previously, a screen for suppressors of activated *goa-1* was performed using heat-shock induced expression of an activated *goa-1* transgene (Hajdu-Cronin *et al.* 1999). This screen isolated many alleles of *dgk-1*, encoding diacyclglycerol kinase, and a single allele of *eat-16*, encoding a regulator of G protein signaling (RGS) protein that negatively regulates G_q (Hajdu-Cronin *et al.* 1999). Because of the strong bias of this screen for isolating alleles of *dgk-1*, we used the *goa-1(n499 ox304*) strain to perform a screen for suppressors of activated G_o that did not involve overexpression of *goa-1*. We performed ENU mutagenesis of *goa-1(n499 ox304*) and isolated F2 animals that were not paralyzed. From a screen of approximately 24,000 mutagenized

haploid genomes, we isolated 17 suppressors, 9 with a relatively stronger suppression phenotype and 8 that were weaker. Of the 9 stronger suppressors, we isolated two alleles of *eat-16* (*ox359*, *ox360*), three alleles of the BK type potassium channel *slo-1* (*ox357*, *ox358*, *ox368*), one allele of the gap junction innexin *unc-9* (*ox353*), one gain-of-function allele in the ion channel gene *nca-1* (*ox352*), and two mutants that were not assigned to genes (*ox356*, *ox364*).

Mapping and cloning *nlf-1(ox327)*

We mapped the *ox327* mutation using single nucleotide polymorphisms (SNPs) in the Hawaiian strain CB4856 as described (Davis et al., 2005). *ox327* was mapped to an approximately 459 kb region on the left arm of the X chromosome between SNPs on cosmids F39H12 and C52B11 (SNPs F39H12[4] and pkP6101). This region included 74 predicted protein-coding genes. We injected cosmids spanning this region and found that cosmid F55A4 rescued the *ox327* mutant phenotype. We performed RNAi to the genes on this cosmid in the *eri-1(mg366) lin-15(n744)* strain that has enhanced RNAi and found that RNAi of the gene F55A4.2 caused a weak fainter phenotype. We sequenced F55A4.2 in the *ox327* mutant and found a T to A transversion mutation in exon 1, leading to a stop codon at amino acid C59. We also rescued the *ox327* mutant with a transgene carrying only F55A4.2. We subsequently obtained a deletion allele *tm3631* that has fainter and G_q suppression phenotypes indistinguishable from *ox327*. F55A4.2 was given the gene name *nlf-1* (Xie *et al.* 2013).

We obtained six independent *nlf-1* cDNAs that were predicted to be full-length: yk1105g4, yk1159a2, yk1188d11, yk1279a1, yk1521f8, and yk1709b10. Restriction digests suggested that all six were of the same size. We sequenced yk1159a2 and yk1279a1 and both gave the same *nlf-1* exon-intron structure, which differed from the gene-structure on Wormbase WS253 in several ways: *nlf-1* is 4 bp shorter at the 3' end of exon 5, and has a new 154 bp exon (now exon 6) not predicted on Wormbase. *nlf-1* consists of 8 exons and is predicted to encode a protein of 438

amino acids (Figure 3A). This is identical to the gene structure reported independently (Xie *et al.* 2013). Both sequenced cDNAs had 5'UTRs of 64 bp, with yk1159a2 (but not yk1279a1) being trans-spliced to the SL1 splice leader, and 3'UTRs of 424 bp (yk1279a1) or 429 bp (yk1159a2). The yk1279a1 cDNA was mutation-free and was cloned into a Gateway entry vector for rescue experiments. The full-length sequence of the yk1279a1 *nlf-1* cDNA was deposited in GenBank under accession # KX808524.

Mapping and cloning *unc-109(n499)*

unc-109 was shown to be allelic to *goa-1*. First, we performed SNP mapping of both *unc-109(n499)* and its intragenic revertant *unc-109(n499 ox303)*, using the Hawaiian strain CB4856 (Davis *et al.* 2005). These experiments mapped *unc-109* to an approximately 1 Mb region in the middle of chromosome I between SNPs on cosmids D2092 and T24B1 (SNPs CE1-15 and T24B1[1]). A good candidate in this region was *goa-1*. We showed that *unc-109* is *goa-1* by sequencing the three *unc-109* mutants: the gain-of-function allele *n499* carries a point mutation that leads to an R179C missense mutation, affecting a conserved arginine residue shown to be important for the GTPase activity of G proteins (Coleman *et al.* 1994); the partial loss-of-function allele *ox304* carries a point mutation leading to a W259R missense mutation; and the strong loss-of-function allele *ox303* carries a one basepair deletion that leads to a stop codon 32 amino acids from the C-terminal.

Molecular biology and transgenes

A complete list of constructs is provided in the plasmid list (Table S2). Most of the constructs were made using the three-slot multisite Gateway system (Invitrogen). For C3 transferase constructs, a promoter, an FRT-mCherry-FRT-GFP cassette (pWD178), and the *C. botulinum* C3 transferase-*unc-54* 3'UTR (cloned into a Gateway entry vector from plasmid QT#99)

were combined into the pDEST R4-R3 destination vector. For *nlf-1* tissue-specific rescue constructs, a promoter, the *nlf-1* coding sequence (genomic DNA or cDNA), and a C-terminal GFP tag were cloned along with the *unc-54* 3'UTR into the pDEST R4-R3 destination vector. Promoters used were *nlf-1p* (5.7 kb upstream of the ATG), *rab-3p* (all neurons), *unc-17p* (acetylcholine neurons), *unc-17Hp* (head acetylcholine neurons) (Hammarlund *et al.* 2007), *acr-2p* (acetylcholine motor neurons), *unc-17βp* (acetylcholine motor neurons) (Charlie *et al.* 2006), and *glr-1p* (glutamate-receptor interneurons). Extrachromosomal arrays were made by standard transformation methods (Mello *et al.* 1991). Constructs of interest were injected at 10 ng/μl with marker and carrier DNAs added to make a final total concentration of at least 100 ng/μl. For most constructs, we isolated multiple independent insertions that behaved similarly. C3 transferase extrachromosomal arrays were integrated into the genome using X-ray irradiation (4000 rads). Integrated transgenes were mapped to chromosomes and outcrossed twice.

Locomotion assays

We performed two different assays to measure locomotion. Body bend assays measured the rate of locomotion. Radial locomotion assays measured the radial distance animals moved from a point in a given unit of time, which provides a combined measurement of different aspects of locomotion including the rate of locomotion, waveform, and frequency of reversals. Both types of assays were performed on 10 cm plates seeded with thin lawns of OP50 bacteria. Plates were prepared by seeding 1.5 ml of stationary phase OP50 bacteria to cover the plate surface and growing the bacteria for two days at room temperature. Seeded plates were stored at 4° for up to one month. For body bend assays, first-day adult worms were picked to an assay plate, allowed to rest for 30 seconds, and then body bends were counted for one minute. A body bend was defined as the movement of the worm from maximum to minimum amplitude of the sine wave (Miller *et al.* 1999). To minimize variation, all animals in an experiment were assayed on the same plate. For

radial locomotion assays, five to eight first-day adults were picked together to the center of a plate to begin the assay (time 0). Positions of the worms were marked on the lid of the plate every ten minutes for up to forty minutes. Following the assay, the distance of each point to the center was measured. For most strains, radial distances did not increase after the first ten minutes of the assay and all data presented here are for the ten-minute time point. For all locomotion assays, the experimenter was blind to the genotypes of the strains assayed.

For Rho inhibition experiments (Figure 1), expression of C3 transferase (C3T) was induced by FLP-mediated recombination. Expression of FLP was induced by heat shock for 1 hr at 34°C, plates were returned to room temperature, and animals were scored for locomotion 4 hrs after the end of the heat shock period. For heat-shock induction of activated Rho (Figure 8), worms were heat shocked for 1 hr at 34°C, returned to room temperature, and scored for locomotion 2 hrs after the end of the heat-shock period.

Fainting assays

Backward fainting times were measured by touching a worm on the head with a worm pick to stimulate movement and measuring the time to faint with a stopwatch. Forward fainting time was measured following a touch on the tail. Fainting was defined by an abrupt stop of movement along with a characteristic straightening of the head (Figure 6A). Alternatively, we touched worms on the head or tail with a pick and counted the number of body bends until the worm fainted. If a worm moved 10 body bends without fainting, we stopped the assay.

Waveform quantification

To quantify the track waveform, first-day adult animals were placed on an OP50 plate and allowed to move forward for a few seconds. We then imaged each animal's tracks using a Nikon SMZ18 microscope with the DS-L3 camera control system. Track pictures were taken at 40X and

were processed using ImageJ. Period and 2X amplitude were measured using the line tool. For each worm, five period/amplitude ratios were averaged. Five individual worms were used per experiment. We present the data for the period/amplitude because this metric is not strongly affected by the size of the animal and thus best captures the exaggerated “loopy” waveform of activated Gq and activated Rho mutants.

The loopy waveform of *egl-30(tg26)* mutants is also characterized by the head of the worm occasionally crossing over the body, leading the worm to form a figure-eight shape (Figure 2A). This phenotype was quantified by placing animals on OP50 plates and allowing them to move forward, counting the number of times the head crossed over the body in one minute.

Imaging and image analysis

Worms were mounted on 2% agarose pads and anesthetized with sodium azide. Images were obtained using a Zeiss Pascal confocal microscope. For quantitative imaging of NCA-1::GFP and NCA-2::GFP (Figure S1), Z-stack projections of the nerve ring axons on one side of the animal were collected and quantified in ImageJ as described (Jospin *et al.* 2007). Dissecting microscope photographs of first-day adult worms were taken at 50X using a Nikon SMZ18 microscope equipped with a DS-L3 camera control system.

Statistics

P values were determined using GraphPad Prism 5.0d (GraphPad Software). Normally distributed data sets with multiple comparisons were analyzed by a one-way ANOVA followed by a Bonferroni or Tukey posthoc test to examine selected comparisons or by Dunnett’s test if all comparisons were to the wild type control. Non-normally distributed data sets with multiple comparisons were analyzed by a Kruskal-Wallis nonparametric ANOVA followed by Dunn’s test to examine selected comparisons. Pairwise data comparisons were analyzed by a two-tailed

unpaired t test for normally distributed data or by a two-tailed Mann-Whitney test for non-normally distributed data.

Reagent and data availability

Strains and plasmids are shown in Table S1 and Table S2 and are available from the *Caenorhabditis* Genetics Center (CGC) or upon request. The full-length sequence of the yk1279a1 *nlf-1* cDNA was deposited in GenBank under accession # KX808524. The authors state that all data necessary for confirming the conclusions presented in the article are represented fully within the article and Supplemental Material.

Results

Inhibition of Rho suppresses activated G_q

Two pieces of data suggested that G_q may regulate locomotion in *C. elegans* through activation of the small G protein Rho. First, both the hyperactive locomotion and tightly-coiled "loopy" body posture of the activated G_q mutant *egl-30(tg26)* are suppressed by loss-of-function mutations in the *unc-73* RhoGEF Trio (Williams *et al.* 2007). Second, expression of activated Rho causes worms to adopt a posture with a tightly-coiled waveform (McMullan *et al.* 2006), reminiscent of the waveform of activated G_q worms (Bastiani *et al.* 2003; Ailion *et al.* 2014). To determine whether G_q signals through Rho, we tested whether Rho inhibition suppresses an activated G_q mutant.

In *C. elegans,* there is a single gene encoding Rho (*rho-1*). Because loss of *rho-1* causes numerous pleiotropic developmental phenotypes and embryonic lethality (Jantsch-Plunger *et al.* 2000), we employed the widely-used Rho inhibitor *Clostridium botulinum* C3 transferase (C3T), which ADP-ribosylates Rho (Aktories *et al.* 2004). C3T has strong substrate specificity for Rho and has only weak activity towards other Rho family members like Rac and Cdc42 (Just *et al.* 1992). Though effects of C3T on targets other than Rho cannot be absolutely excluded, a study in *C. elegans* found that C3T, *rho-1* RNAi, and expression of a dominant-negative form of Rho all caused similar defects in P cell migration (Spencer *et al.* 2001). To bypass the developmental roles and study Rho function in the adult nervous system, we expressed C3T only in adult neurons by using the FLP recombinase/FRT system (Davis *et al.* 2008). In this system, temporal control of C3T is achieved through induction of FLP via heat-shock. FLP in turn promotes recombination between FRT sites to lead to expression of C3 transferase in specific neurons (Figure 1A). We expressed C3T in the following classes of neurons: all neurons (*rab-3p*), acetylcholine neurons *(unc-17p*), head acetylcholine neurons (*unc-17Hp*), and acetylcholine motor

neurons (*unc-17βp*). mCherry fluorescence confirmed expression in the expected neurons and GFP expression was used to monitor induction of C3T following FLP-mediated recombination.

Inhibition of *rho-1* in adult neurons caused a decreased locomotion rate (Figure 1B). This effect was greatest when Rho was inhibited in all neurons, but Rho inhibition in acetylcholine subclasses of neurons also led to slower locomotion. Thus, Rho acts in multiple classes of neurons to promote locomotion in adult worms. In the absence of heat-shock, all strains showed normal wild-type rates of locomotion and did not express any detectable GFP (data not shown), indicating that these transgenes do not provide leaky expression of C3T in the absence of heat-shock. This confirms that Rho acts post-developmentally in mature neurons to regulate locomotion behavior (McMullan *et al.* 2006).

To determine whether Rho acts downstream of G_q signaling, we crossed the C3 transgenes into the background of the activated G_q mutant *egl-30(tg26)*. Inhibition of *rho-1* in all adult neurons suppressed the loopy waveform, body posture, and hyperactive locomotion of the activated G_q mutant (Figure 1, C-F). Inhibition of *rho-1* in acetylcholine neurons suppressed the hyperactivity of activated G_q (Figure 1C), but only weakly suppressed the loopy waveform (Figure 1, D-F). Thus, *rho-1* exhibits genetic interactions consistent with a role in the G_q signaling pathway in both acetylcholine neurons and additional neurons.

Mutations in NCA channel subunits suppress activated G_q

What acts downstream of Rho in the G_q signal transduction pathway? We screened for suppressors of activated G_q and found mutants in three categories: (1) the canonical G_q pathway (such as the PLC *egl-8*); (2) the RhoGEF *unc-73* (Williams *et al.* 2007), and (3) genes that affect dense-core vesicle function (*e.g. unc-31*, *rab-2*, *rund-1*) (Ailion *et al.* 2014; Topalidou *et al.* 2016). Mutations in *unc-73* suppress the loopy waveform of the activated G_q mutant, more strongly than mutations in the canonical G_q pathway or in genes that affect dense-core vesicle function (Figure

2A, C and D). Thus, stronger suppression of the loopy waveform of activated G_q may be a characteristic of mutations in the Rho pathway.

To identify possible downstream targets of Rho in the G_q pathway, we examined other mutants isolated from our screen for suppression of the loopy waveform of activated G_q (Figure 2). When crossed away from the activating G_q mutation, several of these mutants had a "fainter" phenotype. Fainter mutants respond to a touch stimulus by moving away, but abruptly stop, that is "faint", after only a few body bends. The fainter phenotype has been observed only in mutants that reduce the function of the NCA-1 and NCA-2 ion channels (Humphrey *et al.* 2007; Jospin *et al.* 2007; Yeh *et al.* 2008). We found that all our G_q suppressors that strongly suppressed the loopy waveform and had a fainter phenotype were mutants in either *unc-79* or *unc-80*, two genes required for function of the NCA channels (Humphrey *et al.* 2007; Jospin *et al.* 2007; Yeh *et al.* 2008). We also isolated a single mutant in the gene *nlf-1* that also gave fainters after outcrossing away from the activated G_q mutation, but did not strongly suppress the loopy waveform of the activated G_q mutant (Figure 2). *unc-79* and *unc-80* mutants have a strong fainter phenotype equivalent to that of a double mutant in *nca-1* and *nca-2*, two genes that encode pore-forming subunits of the NCA channels in *C. elegans* (Humphrey *et al.* 2007; Jospin *et al.* 2007; Yeh *et al.* 2008). Like *unc-79* or *unc-80*, an *nca-1 nca-2* double mutant suppressed the activated G_q mutant. Additionally, *nca-1* on its own partially suppressed activated G_q, but *nca-2* did not (Figure 2). This suggests that although *nca-1* and *nca-2* are only redundantly required for normal worm locomotion, channels containing the NCA-1 pore-forming subunit have a larger role in transducing G_q signals than NCA-2 channels.

Cloning and characterization of *nlf-1(ox327)*

In addition to the previously known NCA channel subunits *unc-79* and *unc-80*, we also isolated the *ox327* mutant in a gene that had not been previously characterized at the time of our

study. We cloned *ox327* by single nucleotide polymorphism (SNP) mapping, RNAi and transgenic rescue experiments (see Materials and Methods), showing that it carries an early stop mutation in the gene *nlf-1*. We sequenced two *nlf-1* cDNAs and found that its exon-intron structure differed from the gene structure predicted on Wormbase (Figure 3A, see Materials and Methods for details). *nlf-1* was independently cloned by others (Xie *et al.* 2013).

nlf-1 encodes an endoplasmic reticulum-localized protein probably involved in proper assembly of the NCA channel, since *nlf-1* mutants had reduced expression levels of GFP-tagged NCA-1 and NCA-2 (Xie *et al.* 2013). We also found that *nlf-1* is required for normal axonal levels of both GFP-tagged NCA-1 and NCA-2 in the nerve ring (Figure S1). Additionally, an *nlf-1* mutation suppressed both the coiled posture and slow locomotion of an activated *nca-1* mutant (Figure 3, B-F), demonstrating that *nlf-1* is important for NCA-1 function.

nlf-1 mutants have a weaker fainter phenotype than mutants of *unc-79* or *unc-80*, or the *nca-1 nca-2* double mutant (Figure 4, A and B), suggesting that *nlf-1* mutations cause a partial loss of function of the NCA channels. The *nlf-1* fainting phenotype differs in two ways from those of the stronger fainting mutants. First, *nlf-1* mutants take a longer time to faint following stimulation (Figure 4, A and B). Second, while the strong fainting mutants show a similarly strong fainting phenotype in either the forward or backward direction, *nlf-1* mutants faint reliably in the backward direction but have more variable fainting in the forward direction (Figure 4, A and B). Moreover, the *nlf-1(ox327)* mutation did not enhance the *unc-79* or *unc-80* fainter phenotype, suggesting that these mutants act in the same pathway to control fainting (Figure 4, C and D). However, *nca-1* strongly enhanced the *nlf-1* fainter phenotype, but *nca-2* did not significantly enhance *nlf-1* (Figure 4, A and B). Neither *nca-1* nor *nca-2* single mutants have a fainter phenotype on their own (Humphrey *et al.* 2007), but the fact that an *nca-1 nlf-1* double mutant has a strong fainter phenotype suggests that either *nca-1* contributes more than *nca-2* for normal locomotion or that

nlf-1 specifically perturbs function of *nca-2*. Our data presented below are more consistent with the possibility that *nca-1* contributes more than *nca-2* to wild-type locomotion behavior.

We determined the cellular expression pattern of *nlf-1* by fusing its promoter to GFP. *nlf-1p::GFP* was expressed in most or all neurons, but was not detected in other tissues (Figure 5A). This agrees with the expression pattern reported elsewhere (Xie *et al.* 2013). To determine the neuronal focus of the fainter phenotype, we performed rescue experiments in which we determined whether an *nlf-1* mutant could be rescued by expression of a wild-type *nlf-1* cDNA under the control of neuron-specific promoters. Expression of *nlf-1(+)* in all neurons (using the *rab-3* promoter) or acetylcholine neurons (using the *unc-17* promoter) fully rescued the *nlf-1* mutant fainter phenotype (Figure 5B). Expression in acetylcholine motor neurons (using the *acr-2* or *unc-17β* promoters) did not rescue the fainter phenotype, but expression driven by a head-specific derivative of the *unc-17* promoter (*unc-17Hp*) fully rescued the fainter phenotype, indicating that the action of *nlf-1* in head acetylcholine neurons is sufficient to prevent fainting (Figure 5B).

Previously, it was reported that expression of *nlf-1* in premotor interneurons is sufficient to rescue the *nlf-1* mutant fainter phenotype (Xie *et al.* 2013). However, we found that *nlf-1* mutant animals expressing *nlf-1* in premotor interneurons using the *glr-1* promoter (*glr-1p*) had sluggish movement and stopped frequently, though generally not with the characteristic posture typical of fainters, and we saw only weak rescue in our quantitative fainting assays that was not statistically significant (Figure 5C). When we instead measured fainting as the percentage of animals that fainted within ten body bends, we did see a marginally significant rescue by *glr-1* promoter expression (backward fainting: *nlf-1* = 92%, *nlf-1; glr-1p::nlf-1(+)* = 68%, P=0.0738, Fisher's exact test; forward fainting: *nlf-1* = 80%, *nlf-1; glr-1p::nlf-1(+)* = 48%, P=0.0378, Fisher's exact test). We may be underestimating the rescue of the fainting phenotype by *glr-1* promoter expression due to the difficulty distinguishing the frequent pausing from true fainting. Nevertheless, rescue of the *nlf-1* mutant is clearly stronger by expression in head acetylcholine neurons using the *unc-17H*

promoter (Figure 5B). Though our data seem to contradict the previous study reporting that *nlf-1* acts in premotor interneurons (Xie *et al.* 2013), there are several possible explanations. First, like our data, the data in the previous study in fact showed only partial rescue of fainting behavior by expression in premotor interneurons (Xie *et al.* 2013). Second, the premotor interneuron promoter combination used in the previous study (*nmr-1p* + *sra-11p*) leads to expression in several other head interneurons that may contribute to the phenotype. Third, it is possible that rescue is sensitive to expression level and that different levels of expression were achieved in the two studies, leading to different levels of rescue. We conclude that NLF-1 acts in head acetylcholine neurons, including the premotor interneurons, to promote sustained locomotion in the worm. Consistent with this, the premotor command interneurons have recently been shown to use acetylcholine as a neurotransmitter (Pereira *et al.* 2015).

Mutations in NCA channel subunits suppress activated Rho

To determine whether NCA mutants act downstream of Rho, we took advantage of an activated Rho mutant (G14V) expressed specifically in the acetylcholine neurons (McMullan *et al.* 2006). Like an activated G_q mutant, this activated Rho mutant has a loopy waveform. We built double mutants of the activated Rho mutant with mutations in *unc-79*, *unc-80*, *nlf-1* and mutations in the NCA channel genes *nca-1* and *nca-2*. We found that the loopy waveform caused by activated Rho was suppressed in *unc-80* mutants, as well as in *nca-1 nca-2* double mutants (Figure 6). In both cases, the resulting double or triple mutants had a fainter phenotype like the *unc-80* or *nca-1 nca-2* mutants on their own. By contrast, the loopy waveform of activated Rho was incompletely suppressed by a mutation in *nlf-1*, consistent with the *nlf-1* mutation causing only a partial loss of NCA channel function (Figure 6). Reciprocally, activated Rho suppressed the weak fainter phenotype of an *nlf-1* mutant, again because Rho can act on NCA even in the absence of *nlf-1*. Additionally, a mutation in *nca-1* also partially suppressed the loopy waveform of

activated Rho, but a mutation in *nca-2* did not (Figure 6). Thus, channels containing the NCA-1 pore-forming subunit have a larger role than NCA-2 channels in transducing Rho signals, similar to the interaction of NCA-1 and G_q signaling.

Because an activated Rho mutant has slow locomotion (Figure 7A) and *unc-79*, *unc-80*, and *nca-1 nca-2* double mutants also have slow locomotion, it is difficult to determine whether these NCA channel mutants suppress the locomotion phenotype of activated Rho in addition to its waveform. We performed radial locomotion assays that provide a combined measurement of several aspects of the locomotion phenotype, including the rate of movement and loopiness of the waveform (see Materials and Methods). By these assays, mutations in *unc-80* or *nca-1 nca-2* lead to only small increases in the radial distance traveled by an activated Rho mutant and an *nca-2* mutant had no effect (Figure 7B). However, a mutation in *nlf-1* much more strongly increased the radial distance traveled by an activated Rho mutant. Because the *nlf-1* mutant is not as slow on its own, we could also directly assay its effect on the rate of locomotion of an activated Rho mutant by counting the number of body bends per minute. An *nlf-1* mutation strongly increased the rate of locomotion of an activated Rho mutant (Figure 7A). In fact, the *nlf-1* double mutant with activated Rho had a faster rate of locomotion than either activated Rho or *nlf-1* on its own, similar to the effect of *nlf-1* on the locomotion of an activated *nca-1* mutant (Figure 3E). Additionally, a mutation in *nca-1* strongly increased the locomotion rate of the activated Rho mutant, but a mutation in *nca-2* had no effect (Figure 7A), further supporting the idea that NCA channels consisting of the NCA-1 subunit act downstream of G_q and Rho.

Rho regulates worm locomotion independently of effects on development, as demonstrated by the fact that heat-shock induction of an activated Rho transgene in adults leads to a loopy waveform similar to that seen in worms that express activated Rho in acetylcholine neurons (McMullan *et al.* 2006). Consistent with the idea that NCA-1 acts downstream of Rho, mutations in the fainter genes *unc-80* and *nlf-1* suppress the loopy waveform phenotype of heat-shock induced

activated Rho (Figure 8, A-C). Additionally, *nlf-1* also suppresses the locomotion defect of heat-shock induced activated Rho (Figure 8D). Thus, Rho regulates worm locomotion via the NCA channels by acting in adults.

A dominant NCA-1 mutation suppresses activated G_o

In *C. elegans*, the G_q pathway is opposed by signaling through the inhibitory G_o protein GOA-1 (Hajdu-Cronin *et al.* 1999; Miller *et al.* 1999). Thus, loss-of-function mutants in *goa-1* are hyperactive and have a loopy waveform, similar to the gain-of-function G_q mutant *egl-30(tg26)*. We found that the uncloned dominant mutant *unc-109(n499)* which is paralyzed and resembles loss-of-function mutants in *egl-30* (Park and Horvitz 1986) carries an activating mutation in *goa-1* (see Materials and Methods). The *goa-1(n499)* mutant is paralyzed as a heterozygote, and is lethal as a homozygote (Park and Horvitz 1986). We performed a screen for suppressors of *goa-1(n499)* and isolated a partial intragenic suppressor, *goa-1(n499 ox304*) (Materials and Methods). *goa-1(n499 ox304)* homozygote animals are viable but show very little spontaneous movement, with a straight posture and relatively flat waveform (Figure 9, C and D). However, when stimulated, the *goa-1(n499 ox304)* mutant is capable of slow coordinated movements (Figure 9, A and B).

We mutagenized the *goa-1(n499 ox304*) strain and screened for animals that were not paralyzed or did not have a straight posture. Among the suppressors, we isolated a mutant (*ox352*) that was found to be a dominant gain-of-function mutation in the *nca-1* gene (Bend *et al.* 2016). The *nca-1(ox352)* mutant has a coiled posture and loopy waveform reminiscent of the activated G_q and activated Rho mutants (Figure 3B). Furthermore*, nca-1(ox352*) suppresses the straight waveform of the activated G_o mutant *goa-1(n499 ox304)* (Figure 9, C and D). Thus, activation of NCA-1 suppresses activated G_o whereas loss of NCA-1 suppresses activated G_q,

both consistent with the model that G_o inhibits G_q and that NCA-1 is a downstream effector of the G_q pathway.

Discussion

In this study, we identify the NCA-1 and NCA-2 ion channels as downstream effectors of the heterotrimeric G proteins G_q and G_o. G_q activates the RhoGEF Trio and the small GTPase Rho. Rho then acts via an unknown mechanism to activate the NCA-1 and NCA-2 ion channels, which are required for normal neuronal activity and synaptic transmission in *C. elegans* (Jospin *et al.* 2007; Yeh *et al.* 2008; Xie *et al.* 2013; Gao *et al.* 2015). Thus, this work identifies a new genetic pathway from G_q to an ion channel that regulates neuronal excitability and synaptic release: G_q → RhoGEF → Rho → NCA channels (Figure 10). The NCA channels have not been previously identified as effectors of the G_q pathway, so this pathway may give insight into how the NCA channels are activated or regulated.

Previously, it has been demonstrated that activation of $G_o\alpha$ GOA-1 activates the RGS protein EAT-16, which in turn inhibits $G_q\alpha$ (Hajdu-Cronin *et al.* 1999; Miller *et al.* 1999). Loss of *goa-1* leads to hyperactive worms (Mendel *et al.* 1995; Ségalat *et al.* 1995). Here we identified an activated mutation in *goa-1* that causes animals to be paralyzed, closely resembling null mutations in the $G_q\alpha$ gene *egl-30* (Brundage *et al.* 1996). Suppressors of activated G_o include loss-of-function mutations in the RGS EAT-16, and gain-of-function mutations in the NCA-1 channel, suggesting that activated G_o inactivates G_q, and could thereby indirectly inactivate the NCA-1 cation channel. Previously, it has been shown that lack of the depolarizing NCA cation currents can be suppressed by a compensatory loss of the hyperpolarizing potassium current from SLO-1 (Kasap *et al.* 2017), or by loss of the gap junction proteins UNC-9 or UNC-7 (Sedensky and Meneely 1987; Morgan and Sedensky 1995; Bouhours *et al.* 2011). This is consistent with our isolation of *slo-1* and *unc-9* mutants as suppressors of activated G_o, since activation of G_o also leads to reduced NCA activity.

Mutations that eliminate the NCA channels, such as *unc-80* or the *nca-1 nca-2* double mutant, suppress the locomotion and body posture phenotypes of an activated Rho mutant

(Figures 6-8), suggesting that NCA channels act downstream of Rho in a linear pathway. Additionally, channels composed of the pore-forming subunit NCA-1 may be the main targets of G_q-Rho signaling. First, loss-of-function mutations in *nca-1* alone, but not *nca-2*, partially suppress activated G_q and activated Rho mutants. Second, activating gain-of-function mutants of *nca-1* have phenotypes reminiscent of activated G_q and activated Rho mutants, but no activated mutants in *nca-2* have been isolated. Third, loss-of-function mutations in *nca-1*, but not *nca-2*, enhance the weaker fainting phenotype of an *nlf-1* mutant which does not fully eliminate function of the NCA channels. Together these data suggest that although either NCA-1 or NCA-2 activity is sufficient for wild-type locomotion, NCA-1 is likely to be the main target of G protein regulation.

We characterized three locomotory behaviors in this manuscript: locomotion rate, waveform, and fainting. The G_q-Rho-NCA pathway regulates all three behaviors, but our genetic epistasis and cell-specific rescue experiments suggest that these behaviors are differentially regulated and involve at least partially distinct sets of neurons. First, the hyperactive locomotion and loopy waveform phenotypes of the activated G_q mutant are genetically separable, since they are differentially suppressed by mutations in the PLCβ pathway and the Rho-NCA pathway. Mutations in the Rho-NCA pathway suppress both the locomotion rate and loopy waveform of activated G_q whereas mutations in the PLCβ pathway suppress the locomotion rate but only very weakly suppress the loopy waveform of activated G_q. Thus, G_q acts through both the PLCβ pathway and the Rho-NCA pathway to regulate locomotion rate, but primarily through the Rho-NCA pathway to regulate the waveform of the animal. Second, we found that NLF-1 activity in head acetylcholine neurons is sufficient to fully rescue the fainting phenotype of an *nlf-1* mutant. However, inhibition of Rho in the head acetylcholine neurons did not suppress the loopy waveform of the activated G_q mutant, but inhibition of Rho in all neurons did suppress. This suggests that Rho does not act solely in head acetylcholine neurons to regulate the waveform. Thus, the G_q-

Rho-NCA pathway acts in at least two different classes of neurons to regulate fainting and waveform.

It is not clear whether Rho activation of the NCA channels is direct or indirect. G_q directly interacts with and activates the RhoGEF and Rho, as shown by the crystal structure of a complex between $G_q\alpha$, RhoGEF, and Rho (Lutz *et al.* 2007). Rho is known to have many possible effectors and actions in cells (Etienne-Manneville and Hall 2002; Jaffe and Hall 2005). In *C. elegans* neurons, Rho has been previously shown to regulate synaptic transmission via at least two pathways, one involving a direct interaction of Rho with the DAG kinase DGK-1 and one that is DGK-1 independent (McMullan *et al.* 2006). A candidate for the link between Rho and NCA is the type I phosphatidylinositol 4-phosphate 5-kinase (PIP5K) that synthesizes the lipid phosphatidylinositol 4,5,-bisphosphate (PIP2). PIP5K is an intriguing candidate for several reasons. First, activation of G_q in mammalian cells has been shown to stimulate the membrane localization and activity of PIP5K via a mechanism that depends on Rho (Chatah and Abrams 2001; Weernink *et al.* 2004). Second, in *C. elegans*, mutations eliminating either the NCA channels (*nca-1 nca-2* double mutant) or their accessory subunits (*unc-79* or *unc-80*) suppress mutants in the PIP2 phosphatase synaptojanin (*unc-26*) and also suppress phenotypes caused by overexpression of the PIP5K gene *ppk-1* (Jospin *et al.* 2007). Loss of a PIP2 phosphatase or overexpression of a PIP5K are both predicted to increase levels of PIP2. Because the loss of NCA channels suppresses the effects of too much PIP2, it is possible that excessive PIP2 leads to overactivation of NCA channels and that PIP2 might be part of the normal activation mechanism. There are numerous examples of ion channels that are regulated or gated by phosphoinositide lipids such as PIP2 (Balla 2013), though PIP2 has not been shown to directly regulate NCA/NALCN.

The NCA/NALCN ion channel was discovered originally by bioinformatic sequence analyses (Lee *et al.* 1999; Littleton and Ganetzky 2000). It is conserved among all metazoan

animals and is evolutionarily-related to the family of voltage-gated sodium and calcium channels (Liebeskind *et al.* 2012), forming a new branch in this super-family. Although the cellular role of the NCA/NALCN channel and how it is gated are not well understood, NALCN and its orthologs are expressed broadly in the nervous system in a number of organisms (Lee *et al.* 1999; Lear *et al.* 2005; Humphrey *et al.* 2007; Lu *et al.* 2007; Jospin *et al.* 2007; Yeh *et al.* 2008; Lu and Feng 2011; Lutas *et al.* 2016). Moreover, mutations in this channel or its auxiliary subunits lead to defects in rhythmic behaviors in multiple organisms (Lear *et al.* 2005, 2013; Lu *et al.* 2007; Jospin *et al.* 2007; Yeh *et al.* 2008; Pierce-Shimomura *et al.* 2008; Xie *et al.* 2013; Funato *et al.* 2016). Thus, NCA/NALCN is likely to play an important role in controlling membrane excitability. Additionally, NALCN currents have been reported to be activated by two different G protein-coupled receptors (GPCRs), the muscarinic acetylcholine receptor and the substance P receptor, albeit in a G protein-independent fashion (Lu *et al.* 2009; Swayne *et al.* 2009), and by low extracellular calcium via a G protein-dependent pathway (Lu *et al.* 2010). The latter study further showed that expression of an activated G_q mutant inhibited the NALCN sodium leak current, suggesting that high extracellular calcium tonically inhibits NALCN via a G_q-dependent pathway and that low extracellular calcium activates NALCN by relieving this inhibition (Lu *et al.* 2010). By contrast, we find that G_q activates the NCA channels in *C. elegans*, and we show that the NCA channels are physiologically relevant targets of a G_q signaling pathway that acts through Rho.

In the last few years, both recessive and dominant human diseases characterized by a range of neurological symptoms including hypotonia, intellectual disability, and seizures have been shown to be caused by mutations in either *NALCN* or *UNC80* (Köroğlu *et al.* 2013; Al-Sayed *et al.* 2013; Chong *et al.* 2015; Aoyagi *et al.* 2015; Shamseldin *et al.* 2016; Stray-Pedersen *et al.* 2016; Gal *et al.* 2016; Fukai *et al.* 2016; Karakaya *et al.* 2016; Perez *et al.* 2016; Bend *et al.* 2016; Lozic *et al.* 2016; Valkanas *et al.* 2016; Wang *et al.* 2016; Vivero *et al.* 2017). Notably, dominant disease-causing mutations in the NALCN channel were modeled in worms and resemble either

dominant activated or loss-of-function NCA mutants such as the ones we use in this study (Aoyagi *et al.* 2015; Bend *et al.* 2016). Human mutations in other components of the pathway we have described may cause similar clinical phenotypes.

Acknowledgments

We thank Shohei Mitani for the *nlf-1(tm3631)* mutant; Steve Nurrish for worm strains and plasmids carrying activated Rho or C3 transferase; Ken Miller for a plasmid with the *unc-17β* promoter; Wayne Davis for FLP/FRT plasmids; Yuji Kohara for cDNA clones; the Sanger Center for cosmids; Brooke Jarvie, Jill Hoyt, and Michelle Giarmarco for the isolation of *unc-79* and *unc-80* mutations in the G_q suppressor screen; and Dana Miller for the use of her microscope and camera to take worm photographs. Some strains were provided by the CGC, which is funded by NIH Office of Research Infrastructure Programs (P40 OD010440). M.A. is an Ellison Medical Foundation New Scholar. E.M.J. is an Investigator of the Howard Hughes Medical Institute. This work was supported by NIH grants R00 MH082109 to M.A and R01 NS034307 to E.M.J.

Figure Legends

Figure 1 Inhibition of Rho in neurons suppresses an activated G_q mutant. (A) Schematic of the FLP/FRT system we used for temporal and spatial expression of the Rho inhibitor C3 transferase (C3T). The transgene in the ‘‘off’’ configuration expresses the mCherry reporter under the control of the promoter sequence but terminates transcription in the *let-858* 3’UTR upstream of GFP-C3T. Expression of the FLP recombinase is induced by heat shock and leads to recombination between the FRT sites and deletion of the intervening *mCherry::let-858* 3’UTR fragment. This leads to transcription of GFP-C3T in the cells driven by the adjacent promoter. We used the pan-neuronal promoter *rab-3p,* acetylcholine neuron promoter *unc-17p,* and head acetylcholine neuron promoter *unc-17Hp.* (B) Inhibition of Rho by C3 transferase (C3T) in all adult neurons (*rab-3p, oxIs412* transgene), acetylcholine neurons (*unc-17p, oxIs414* transgene) or head acetylcholine neurons (*unc-17Hp, oxIs434* transgene) reduces the locomotion rate of wild type animals. ***, P<0.001, Dunnett’s test. Error bars = SEM; n = 19-20. (C) Inhibition of Rho in all adult neurons (*rab-3p, oxIs412* transgene) or acetylcholine neurons (*unc-17p*, *oxIs414* transgene) leads to a significant reduction in the rate of locomotion of the activated G_q mutant *egl-30(tg26)* (here written Gq*). Inhibition of Rho in head acetylcholine neurons (*unc-17Hp*, *oxIs434* transgene) leads to a small decrease in Gq* locomotion that is not statistically significant. ***, P<0.001; ns, not significant, P>0.05, Dunnett’s test. Error bars = SEM; n = 10-20. (D) Photos of first-day adult worms. The coiled body posture of the activated G_q mutant *egl-30(tg26)* (Gq*) is suppressed by Rho inhibition in all neurons (*rab-3p::C3T*). (E) Photos of worm tracks. (F) Quantification of the track waveform. The loopy waveform of the activated G_q mutant *egl-30(tg26)* (Gq*) is suppressed by Rho inhibition in all adult neurons (*rab-3p::C3T*) and partially suppressed by Rho inhibition in acetylcholine neurons (*unc-17p::C3T*). Rho inhibition in head acetylcholine (*unc-17Hp::C3T*)

neurons does not suppress the loopy waveform of Gq*. ***, P<0.001; ns, not significant, P>0.05, Bonferroni test. All comparisons are to Gq*. Error bars = SEM; n = 5.

Figure 2 Mutations affecting the NCA-1 and NCA-2 channels suppress the loopy waveform of the activated G_q mutant *egl-30(tg26)* (Gq*). (A) Photos of first-day adults. The *unc-73(ox317)*, *unc-79(yak37),* and *unc-80(ox330)* mutations suppress the loopy waveform of Gq*. (B) Photos of worm tracks. The photo of wild type tracks is the same as the one shown in Figure 3C. (C) Quantification of the track waveform. The wild-type waveform data are the same data shown in Figures 3D, 6C, and 9D. (D) Quantification of the worm's head crossing its body ("crossovers"). The *nca-1(gk9)* and *nlf-1(ox327)* mutations partially suppress the loopy waveform of Gq* as measured by the crossover assay. Mutations in the canonical G_q pathway such as *egl-8(ox333)* partially suppress and genes required for dense-core vesicle biogenesis such as *rund-1(tm3622)* do not significantly suppress the loopy waveform of Gq*. The *nca-2(gk5)* mutation does not suppress Gq*. ***, P<0.001; **, P<0.01; *, P<0.05; ns, not significant, P>0.05, Bonferroni test. All comparisons are to Gq*. Error bars = SEM; n = 5 (panel C); n = 6 (panel D).

Figure 3 The *nlf-1(ox327)* mutation suppresses the coiled posture, loopy waverform, and locomotion defect of the activated NCA-1 mutant *nca-1(ox352*) (Nca*). (A) Gene structure of *nlf-1*. Black boxes show coding segments. White boxes show 5' and 3' untranslated regions (UTRs). The *ox327* mutation leads to a premature stop codon at C59. The *tm3631* deletion removes most of the 5'UTR and first exon. (B) Photos of first-day adult worms. (C) Photos of worm tracks. The photo of wild type tracks is the same as the one shown in Figure 2B. (D) Quantification of track waveform. The loopy waveform of Nca* is suppressed by *nlf-1.* The wild-type data are the same data shown in Figures 2C, 6C, and 9D. (E) Body bend assay. The wild-type data shown in the left graph are the same as shown in Figure 7A, right graph. (F) Radial locomotion assay. Statistics in

D: ***, P<0.001, two-tailed unpaired t test. Comparisons are to Nca*. Error bars = SEM, n = 5. Statistics in E and F: ***, P<0.001, two-tailed Mann-Whitney test. Error bars = SEM, n = 4-10 (panel E), n = 8-26 (panel F).

Figure 4 *nlf-1* mutants are weak fainters. The *nlf-1(ox327)* mutant is a weaker fainter in the forward direction (A) than the backward direction (B), but *nlf-1(ox327)* has a weaker fainter phenotype than either *unc-80(ox330)* or the *nca-2(gk5)*; *nca-1(gk9)* double mutant. Additionally, *nlf-1* mutants are enhanced by a mutation in *nca-1*, but not *nca-2*. Wild-type, *nca-1(gk9)*, and *nca-2(gk5)* mutant animals are not shown in the figure because they do not faint (0/10 animals fainted in a one minute period). Also, *nlf-1(ox327)* mutants do not enhance the strong forward (C) or backward (D) fainting phenotypes of *unc-79(e1068)* and *unc-80(ox330)* mutants. ***, P<0.001; ns, not significant, P>0.05, Dunn's test. Error bars = SEM; n = 10-20.

Figure 5 *nlf-1* acts in head acetylcholine neurons to control locomotion. (A) *nlf-1* is expressed widely in the nervous system. A fusion of the *nlf-1* promoter to GFP (transgene *oxEx1144*) is expressed throughout the nervous system. No expression is seen in non-neuronal tissues. An L1 stage larval animal is shown with its head to the left. (B,C) The *nlf-1* cDNA was expressed in an *nlf-1(ox327)* mutant background using the following promoters: *rab-3* (all neurons, *oxEx1146* transgene), *unc-17* (acetylcholine neurons, *oxEx1149* transgene), *unc-17H* (a derivative of the *unc-17* promoter that lacks the enhancer for ventral cord expression and thus expresses in head acetylcholine neurons and occasionally a few tail neurons, *oxEx1155* transgene), *unc-17*β (a derivative of the *unc-17* promoter that expresses only in ventral cord acetylcholine neurons, *oxEx1323* transgene), *acr-2* (ventral cord acetylcholine motor neurons, *oxEx1151* transgene), and *glr-1* (interneurons including premotor command interneurons, *oxEx1152* transgene). (B) Expression driven by the *rab-3*, *unc-17*, and *unc-17H* promoters rescued the fainting phenotype of

an *nlf-1* mutant in the backward direction. ***, P<0.001, Dunn's test. Error bars = SEM; n = 15. (C) Expression driven by the *glr-1* promoter partially rescued the fainting phenotype of an *nlf-1* mutant in either the backward or forward direction, though the effect was not statistically significant (ns, P>0.05, two-tailed Mann-Whitney tests. Error bars = SEM; n = 25). However, assays of this strain were complicated by slow movement and frequent pauses that were hard to distinguish from true fainting behavior (see text for details).

Figure 6 Mutations in NCA channel subunits suppress the loopy waveform of animals expressing activated Rho. (A) Photos of first-day adult worms. Mutants in *unc-80*, *nlf-1*, and the *nca-2 nca-1* double mutant have the typical fainter posture characterized by a straightened anterior part of the body. Animals expressing an activated Rho mutant (G14V) in acetylcholine neurons (*nzIs29* transgene, written as Rho*) have a loopy waveform. Mutations that eliminate NCA-1 and NCA-2 channel function (*unc-80(ox330)* or *nca-2(gk5)*; *nca-1(gk9)*) suppress the loopy waveform of activated Rho and convert the activated Rho mutants to fainters. Mutations in *nlf-1(ox327)* and *nca-1(gk9)* strongly but incompletely suppress the loopy waveform of activated Rho and these double mutants do not faint. Mutations in *nca-2(gk5)* do not suppress the loopy waveform of activated Rho. (B) Photos of worm tracks. (C) Quantification of track waveform. The wild-type data are the same data shown in Figures 2C, 3D, and 9D. ***, P<0.001; **, P<0.01; ns, not significant, P>0.05, Bonferroni test. All comparisons are to Rho*. Error bars = SEM; n = 5.

Figure 7 Mutations in *nlf-1* and *nca-1* suppress the locomotion defect of animals expressing activated Rho. (A) Animals expressing an activated Rho mutant (G14V) in acetylcholine neurons (*nzIs29* transgene, written as Rho*) have a slow locomotion rate as measured by the number of body bends. The *nlf-1(ox327)* and *nca-1(gk9)* mutations, but not *nca-2(gk5)*, strongly suppress the slow locomotion rate of activated Rho. The wild-type data shown in the right graph are the same

as shown in Figure 3E, left graph. (B) Animals expressing an activated Rho mutant (G14V) in acetylcholine neurons (Rho*) have reduced locomotion as measured in radial locomotion assays. Mutations that eliminate function of the NCA channels (*unc-80(ox330)* or *nca-2(gk5)*; *nca-1(gk9)*) increase the radial distance traveled by activated Rho mutants, but the effect is small since *unc-80* and *nca-2; nca-1* mutants have reduced locomotion on their own. The *nlf-1(ox327)* mutation that partially reduces function of the NCA channels strongly suppresses the locomotion defect of activated Rho. In the particular radial locomotion experiment shown here, only five Rho**; nca-1* animals were assayed and they had a mean radial distance traveled of 2.4 mm, very similar to the mean radial distance of the Rho* single mutant (2.0 mm, n=18). However, in an independent experiment, the Rho**; nca-1* double mutant had a mean radial distance of 12.2 mm (n=10) as compared to 3.5 mm for the Rho* single mutant (n=10). Thus, it is likely that *nca-1* does indeed suppress *Rho** in radial locomotion assays, but gave a negative result in the presented assay due to low n, possibly because these particular Rho*; *nca-1* animals moved outward and returned to the center. ***, P<0.001; ns, not significant, P>0.05, Bonferroni test. Error bars = SEM; n = 10-16 (panel A); n = 5-18 (panel B).

Figure 8 Mutations in NCA channel subunits suppress the loopy waveform and locomotion of adult animals expressing activated Rho. (A) Photos of first-day adult worms. Animals expressing an activated Rho mutant (G14V) only in adults by heat-shock induced expression (*nzIs1* transgene, *hs::Rho**) have a loopy waveform. The *unc-80(ox330)* and *nlf-1(ox327)* mutations strongly suppress the loopy waveform of activated Rho. *unc-80*, but not *nlf-1*, makes the activated Rho animals faint. (B) Photos of worm tracks. (C) Quantification of track waveform. (D) Body bend assay. The *nlf-1(ox327)* mutation suppresses the reduced locomotion rate of activated Rho. Statistics in C: ***, P<0.001, Bonferroni test. Error bars = SEM; n = 5. Statistics in D: *, P=0.0157, two-tailed unpaired t test. Error bars = SEM; n = 18-30.

Figure 9 An activated NCA-1 mutant suppresses the straight posture and relatively flat waveform of an activated GOA-1 mutant. The *goa-1(n499 ox304)* mutant (written as Go*) has a strong movement defect as shown by a body bend assay (A) and a radial locomotion assay (B). ***, P<0.001; **, P<0.01, two-tailed unpaired t-tests. Error bars = SEM; n = 10 (panel A); n = 18 (panel B). Also the *goa-1(n499 ox304)* mutant has a relatively straight posture (C) and flat waveform (D) that is suppressed by the *nca-1(ox352)* mutation (written as Nca*). The wild-type waveform data are the same data shown in Figures 2C, 3D, and 6C. ***, P<0.001; **, P<0.01, Bonferroni test. Comparisons are to Go*. Error bars = SEM; n = 5-6.

Figure 10 Model. G_q activates NCA-1 in a linear pathway via the RhoGEF Trio and small G protein Rho. G_q activation of Trio and Rho is direct (solid arrow). Rho activation of the NCA-1 channel is likely to be indirect (dashed arrow). G_o inhibits G_q via the RGS protein EAT-16 (Hajdu-Cronin *et al.* 1999). Thus, loss-of-function mutations in the channel pore-forming subunit NCA-1, its associated subunits UNC-79 and UNC-80, or the ER-localized NCA channel assembly factor NLF-1 suppress an activated G_q mutant, whereas a gain-of-function activating mutation in NCA-1 suppresses an activated G_o mutant. Though the NCA-1 channel has the greatest role in conveying G_q-Rho signals, channels composed of the NCA-2 pore-forming subunit are also probably regulated by G_q because elimination of both NCA-1 and NCA-2 is required to fully suppress activated G_q and activated Rho mutants.

Literature Cited

Adachi T., Kunitomo H., Tomioka M., Ohno H., Okochi Y. *et al.*, 2010 Reversal of salt preference is directed by the insulin/PI3K and Gq/PKC signaling in Caenorhabditis elegans. Genetics **186**: 1309–1319.

Ailion M., Hannemann M., Dalton S., Pappas A., Watanabe S. *et al.*, 2014 Two Rab2 interactors regulate dense-core vesicle maturation. Neuron **82**: 167–180.

Aktories K., Wilde C., Vogelsgesang M., 2004 Rho-modifying C3-like ADP-ribosyltransferases. Rev. Physiol. Biochem. Pharmacol. **152**: 1–22.

Al-Sayed M. D., Al-Zaidan H., Albakheet A., Hakami H., Kenana R. *et al.*, 2013 Mutations in NALCN cause an autosomal-recessive syndrome with severe hypotonia, speech impairment, and cognitive delay. Am. J. Hum. Genet. **93**: 721–726.

Aoyagi K., Rossignol E., Hamdan F. F., Mulcahy B., Xie L. *et al.*, 2015 A Gain-of-Function Mutation in NALCN in a Child with Intellectual Disability, Ataxia, and Arthrogryposis. Hum. Mutat. **36**: 753–757.

Balla T., 2013 Phosphoinositides: tiny lipids with giant impact on cell regulation. Physiol. Rev. **93**: 1019–1137.

Bastiani C. A., Gharib S., Simon M. I., Sternberg P. W., 2003 Caenorhabditis elegans Galphaq regulates egg-laying behavior via a PLCbeta-independent and serotonin-dependent signaling pathway and likely functions both in the nervous system and in muscle. Genetics **165**: 1805–1822.

Bend E. G., Si Y., Stevenson D. A., Bayrak-Toydemir P., Newcomb T. M. *et al.*, 2016 NALCN channelopathies: Distinguishing gain-of-function and loss-of-function mutations. Neurology **87**: 1131–1139.

Boone A. N., Senatore A., Chemin J., Monteil A., Spafford J. D., 2014 Gd3+ and calcium sensitive, sodium leak currents are features of weak membrane-glass seals in patch clamp recordings. PLoS ONE **9**: e98808.

Bouhours M., Po M. D., Gao S., Hung W., Li H. *et al.*, 2011 A co-operative regulation of neuronal excitability by UNC-7 innexin and NCA/NALCN leak channel. Mol Brain **4**: 16.

Brundage L., Avery L., Katz A., Kim U. J., Mendel J. E. *et al.*, 1996 Mutations in a C. elegans Gqalpha gene disrupt movement, egg laying, and viability. Neuron **16**: 999–1009.

Charlie N. K., Schade M. A., Thomure A. M., Miller K. G., 2006 Presynaptic UNC-31 (CAPS) is required to activate the G alpha(s) pathway of the Caenorhabditis elegans synaptic signaling network. Genetics **172**: 943–961.

Chatah N. E., Abrams C. S., 2001 G-protein-coupled receptor activation induces the membrane translocation and activation of phosphatidylinositol-4-phosphate 5-kinase I alpha by a Rac- and Rho-dependent pathway. J. Biol. Chem. **276**: 34059–34065.

Chong J. X., McMillin M. J., Shively K. M., Beck A. E., Marvin C. T. *et al.*, 2015 De novo mutations in NALCN cause a syndrome characterized by congenital contractures of the limbs and face, hypotonia, and developmental delay. Am. J. Hum. Genet. **96**: 462–473.

Coleman D. E., Berghuis A. M., Lee E., Linder M. E., Gilman A. G. *et al.*, 1994 Structures of active conformations of Gi alpha 1 and the mechanism of GTP hydrolysis. Science **265**: 1405–1412.

Coulon P., Kanyshkova T., Broicher T., Munsch T., Wettschureck N. *et al.*, 2010 Activity Modes in Thalamocortical Relay Neurons are Modulated by G(q)/G(11) Family G-proteins - Serotonergic and Glutamatergic Signaling. Front Cell Neurosci **4**: 132.

Davis M. W., Hammarlund M., Harrach T., Hullett P., Olsen S. *et al.*, 2005 Rapid single nucleotide polymorphism mapping in C. elegans. BMC Genomics **6**: 118.

Davis M. W., Morton J. J., Carroll D., Jorgensen E. M., 2008 Gene activation using FLP recombinase in C. elegans. PLoS Genet. **4**: e1000028.

Esposito G., Amoroso M. R., Bergamasco C., Di Schiavi E., Bazzicalupo P., 2010 The G protein regulators EGL-10 and EAT-16, the Giα GOA-1 and the G(q)α EGL-30 modulate the response of the C. elegans ASH polymodal nociceptive sensory neurons to repellents. BMC Biol. **8**: 138.

Etienne-Manneville S., Hall A., 2002 Rho GTPases in cell biology. Nature **420**: 629–635.

Fukai R., Saitsu H., Okamoto N., Sakai Y., Fattal-Valevski A. *et al.*, 2016 De novo missense mutations in NALCN cause developmental and intellectual impairment with hypotonia. J. Hum. Genet. **61**: 451–455.

Funato H., Miyoshi C., Fujiyama T., Kanda T., Sato M. *et al.*, 2016 Forward-genetics analysis of sleep in randomly mutagenized mice. Nature **539**: 378–383.

Gal M., Magen D., Zahran Y., Ravid S., Eran A. *et al.*, 2016 A novel homozygous splice site mutation in NALCN identified in siblings with cachexia, strabismus, severe intellectual disability, epilepsy and abnormal respiratory rhythm. Eur J Med Genet **59**: 204–209.

Gamper N., Reznikov V., Yamada Y., Yang J., Shapiro M. S., 2004 Phosphatidylinositol 4,5-bisphosphate signals underlie receptor-specific Gq/11-mediated modulation of N-type Ca2+ channels. J. Neurosci. **24**: 10980–10992.

Gao S., Xie L., Kawano T., Po M. D., Pirri J. K. *et al.*, 2015 The NCA sodium leak channel is required for persistent motor circuit activity that sustains locomotion. Nat Commun **6**: 6323.

Hajdu-Cronin Y. M., Chen W. J., Patikoglou G., Koelle M. R., Sternberg P. W., 1999 Antagonism between G(o)alpha and G(q)alpha in Caenorhabditis elegans: the RGS protein EAT-16 is

necessary for G(o)alpha signaling and regulates G(q)alpha activity. Genes Dev **13**: 1780–1793.

Hammarlund M., Palfreyman M. T., Watanabe S., Olsen S., Jorgensen E. M., 2007 Open syntaxin docks synaptic vesicles. PLoS Biol. **5**: e198.

Hiley E., McMullan R., Nurrish S. J., 2006 The Galpha12-RGS RhoGEF-RhoA signalling pathway regulates neurotransmitter release in C. elegans. EMBO J. **25**: 5884–5895.

Humphrey J. A., Hamming K. S., Thacker C. M., Scott R. L., Sedensky M. M. *et al.*, 2007 A putative cation channel and its novel regulator: cross-species conservation of effects on general anesthesia. Curr. Biol. **17**: 624–629.

Jaffe A. B., Hall A., 2005 Rho GTPases: biochemistry and biology. Annu. Rev. Cell Dev. Biol. **21**: 247–269.

Jantsch-Plunger V., Gönczy P., Romano A., Schnabel H., Hamill D. *et al.*, 2000 CYK-4: A Rho family gtpase activating protein (GAP) required for central spindle formation and cytokinesis. J. Cell Biol. **149**: 1391–1404.

Jospin M., Watanabe S., Joshi D., Young S., Hamming K. *et al.*, 2007 UNC-80 and the NCA ion channels contribute to endocytosis defects in synaptojanin mutants. Curr. Biol. **17**: 1595–1600.

Just I., Mohr C., Schallehn G., Menard L., Didsbury J. R. *et al.*, 1992 Purification and characterization of an ADP-ribosyltransferase produced by Clostridium limosum. J. Biol. Chem. **267**: 10274–10280.

Karakaya M., Heller R., Kunde V., Zimmer K.-P., Chao C.-M. *et al.*, 2016 Novel Mutations in the Nonselective Sodium Leak Channel (NALCN) Lead to Distal Arthrogryposis with Increased Muscle Tone. Neuropediatrics **47**:273-277.

Kasap M., Bonnett K., Aamodt E. J., Dwyer D. S., 2017 Akinesia and freezing caused by Na(+) leak-current channel (NALCN) deficiency corrected by pharmacological inhibition of K(+) channels and gap junctions. J. Comp. Neurol. **525**: 1109–1121.

Köroğlu Ç., Seven M., Tolun A., 2013 Recessive truncating NALCN mutation in infantile neuroaxonal dystrophy with facial dysmorphism. J. Med. Genet. **50**: 515–520.

Krause M., Offermanns S., Stocker M., Pedarzani P., 2002 Functional specificity of G alpha q and G alpha 11 in the cholinergic and glutamatergic modulation of potassium currents and excitability in hippocampal neurons. J. Neurosci. **22**: 666–673.

Lackner M. R., Nurrish S. J., Kaplan J. M., 1999 Facilitation of synaptic transmission by EGL-30 Gqalpha and EGL-8 PLCbeta: DAG binding to UNC-13 is required to stimulate acetylcholine release. Neuron **24**: 335–346.

Lear B. C., Lin J.-M., Keath J. R., McGill J. J., Raman I. M. *et al.*, 2005 The ion channel narrow abdomen is critical for neural output of the Drosophila circadian pacemaker. Neuron **48**: 965–976.

Lear B. C., Darrah E. J., Aldrich B. T., Gebre S., Scott R. L. *et al.*, 2013 UNC79 and UNC80, Putative Auxiliary Subunits of the NARROW ABDOMEN Ion Channel, Are Indispensable for Robust Circadian Locomotor Rhythms in Drosophila. PLoS ONE **8**: e78147.

Lee J. H., Cribbs L. L., Perez-Reyes E., 1999 Cloning of a novel four repeat protein related to voltage-gated sodium and calcium channels. FEBS Lett. **445**: 231–236.

Liebeskind B. J., Hillis D. M., Zakon H. H., 2012 Phylogeny unites animal sodium leak channels with fungal calcium channels in an ancient, voltage-insensitive clade. Mol. Biol. Evol. **29**: 3613–3616.

Littleton J. T., Ganetzky B., 2000 Ion channels and synaptic organization: analysis of the Drosophila genome. Neuron **26**: 35–43.

Lozic B., Johansson S., Lovric Kojundzic S., Markic J., Knappskog P. M. *et al.*, 2016 Novel NALCN variant: altered respiratory and circadian rhythm, anesthetic sensitivity. Ann Clin Transl Neurol **3**: 876–883.

Lu B., Su Y., Das S., Liu J., Xia J. *et al.*, 2007 The neuronal channel NALCN contributes resting sodium permeability and is required for normal respiratory rhythm. Cell **129**: 371–383.

Lu B., Su Y., Das S., Wang H., Wang Y. *et al.*, 2009 Peptide neurotransmitters activate a cation channel complex of NALCN and UNC-80. Nature **457**: 741–744.

Lu B., Zhang Q., Wang H., Wang Y., Nakayama M. *et al.*, 2010 Extracellular calcium controls background current and neuronal excitability via an UNC79-UNC80-NALCN cation channel complex. Neuron **68**: 488–499.

Lu T. Z., Feng Z.-P., 2011 A sodium leak current regulates pacemaker activity of adult central pattern generator neurons in Lymnaea stagnalis. PLoS ONE **6**: e18745.

Lutas A., Lahmann C., Soumillon M., Yellen G., 2016 The leak channel NALCN controls tonic firing and glycolytic sensitivity of substantia nigra pars reticulata neurons. eLife **5**: e15271.

Lutz S., Freichel-Blomquist A., Yang Y., Rümenapp U., Jakobs K. H. *et al.*, 2005 The guanine nucleotide exchange factor p63RhoGEF, a specific link between Gq/11-coupled receptor signaling and RhoA. J. Biol. Chem. **280**: 11134–11139.

Lutz S., Shankaranarayanan A., Coco C., Ridilla M., Nance M. R. *et al.*, 2007 Structure of Galphaq-p63RhoGEF-RhoA complex reveals a pathway for the activation of RhoA by GPCRs. Science **318**: 1923–1927.

Matsuki M., Kunitomo H., Iino Y., 2006 Goalpha regulates olfactory adaptation by antagonizing Gqalpha-DAG signaling in Caenorhabditis elegans. Proc. Natl. Acad. Sci. U.S.A. **103**: 1112–1117.

McMullan R., Hiley E., Morrison P., Nurrish S. J., 2006 Rho is a presynaptic activator of neurotransmitter release at pre-existing synapses in C. elegans. Genes Dev. **20**: 65–76.

Mello C. C., Kramer J. M., Stinchcomb D., Ambros V., 1991 Efficient gene transfer in C.elegans: extrachromosomal maintenance and integration of transforming sequences. EMBO J **10**: 3959–3970.

Mendel J. E., Korswagen H. C., Liu K. S., Hajdu-Cronin Y. M., Simon M. I. *et al.*, 1995 Participation of the protein Go in multiple aspects of behavior in C. elegans. Science **267**: 1652–1655.

Miller K. G., Emerson M. D., Rand J. B., 1999 Goalpha and diacylglycerol kinase negatively regulate the Gqalpha pathway in C. elegans. Neuron **24**: 323–333.

Morgan P. G., Sedensky M. M., 1995 Mutations affecting sensitivity to ethanol in the nematode, Caenorhabditis elegans. Alcohol. Clin. Exp. Res. **19**: 1423–1429.

Park E. C., Horvitz H. R., 1986 Mutations with dominant effects on the behavior and morphology of the nematode Caenorhabditis elegans. Genetics **113**: 821–852.

Pereira L., Kratsios P., Serrano-Saiz E., Sheftel H., Mayo A. E. *et al.*, 2015 A cellular and regulatory map of the cholinergic nervous system of C. elegans. eLife **4**: e12432.

Perez Y., Kadir R., Volodarsky M., Noyman I., Flusser H. *et al.*, 2016 UNC80 mutation causes a syndrome of hypotonia, severe intellectual disability, dyskinesia and dysmorphism, similar to that caused by mutations in its interacting cation channel NALCN. J. Med. Genet. **53**: 397–402.

Pierce-Shimomura J. T., Chen B. L., Mun J. J., Ho R., Sarkis R. *et al.*, 2008 Genetic analysis of crawling and swimming locomotory patterns in C. elegans. Proc. Natl. Acad. Sci. U.S.A. **105**: 20982–20987.

Sánchez-Fernández G., Cabezudo S., García-Hoz C., Benincá C., Aragay A. M. *et al.*, 2014 Gαq signalling: the new and the old. Cell. Signal. **26**: 833–848.

Sedensky M. M., Meneely P. M., 1987 Genetic analysis of halothane sensitivity in Caenorhabditis elegans. Science **236**: 952–954.

Ségalat L., Elkes D. A., Kaplan J. M., 1995 Modulation of serotonin-controlled behaviors by Go in Caenorhabditis elegans. Science **267**: 1648–1651.

Senatore A., Monteil A., Minnen J. van, Smit A. B., Spafford J. D., 2013 NALCN ion channels have alternative selectivity filters resembling calcium channels or sodium channels. PLoS ONE **8**: e55088.

Senatore A., Spafford J. D., 2013 A uniquely adaptable pore is consistent with NALCN being an ion sensor. Channels **7**: 60–68.

Shamseldin H. E., Faqeih E., Alasmari A., Zaki M. S., Gleeson J. G. *et al.*, 2016 Mutations in UNC80, Encoding Part of the UNC79-UNC80-NALCN Channel Complex, Cause Autosomal-Recessive Severe Infantile Encephalopathy. Am. J. Hum. Genet. **98**: 210–215.

Spencer A. G., Orita S., Malone C. J., Han M., 2001 A RHO GTPase-mediated pathway is required during P cell migration in Caenorhabditis elegans. Proc. Natl. Acad. Sci. U.S.A. **98**: 13132–13137.

Stray-Pedersen A., Cobben J.-M., Prescott T. E., Lee S., Cang C. *et al.*, 2016 Biallelic Mutations in UNC80 Cause Persistent Hypotonia, Encephalopathy, Growth Retardation, and Severe Intellectual Disability. Am. J. Hum. Genet. **98**: 202–209.

Swayne L. A., Mezghrani A., Varrault A., Chemin J., Bertrand G. *et al.*, 2009 The NALCN ion channel is activated by M3 muscarinic receptors in a pancreatic beta-cell line. EMBO Rep. **10**: 873–880.

Topalidou I., Cattin-Ortolá J., Pappas A. L., Cooper K., Merrihew G. E. *et al.*, 2016 The EARP Complex and Its Interactor EIPR-1 Are Required for Cargo Sorting to Dense-Core Vesicles. PLoS Genet. **12**: e1006074.

Valkanas E., Schaffer K., Dunham C., Maduro V., Souich C. du *et al.*, 2016 Phenotypic evolution of UNC80 loss of function. Am. J. Med. Genet. A **170**: 3106–3114.

Vivero M., Cho M. T., Begtrup A., Wentzensen I. M., Walsh L. *et al.*, 2017 Additional de novo missense genetic variants in NALCN associated with CLIFAHDD syndrome. Clin. Genet. doi: **10.1111/cge.12899**.

Vogt S., Grosse R., Schultz G., Offermanns S., 2003 Receptor-dependent RhoA activation in G12/G13-deficient cells: genetic evidence for an involvement of Gq/G11. J. Biol. Chem. **278**: 28743–28749.

Wang Y., Koh K., Ichinose Y., Yasumura M., Ohtsuka T. *et al.*, 2016 A de novo mutation in the NALCN gene in an adult patient with cerebellar ataxia associated with intellectual disability and arthrogryposis. Clin. Genet. **90**: 556–557.

Weernink P. A. O., Meletiadis K., Hommeltenberg S., Hinz M., Ishihara H. *et al.*, 2004 Activation of type I phosphatidylinositol 4-phosphate 5-kinase isoforms by the Rho GTPases, RhoA, Rac1, and Cdc42. J. Biol. Chem. **279**: 7840–7849.

Wilkie T. M., Scherle P. A., Strathmann M. P., Slepak V. Z., Simon M. I., 1991 Characterization of G-protein alpha subunits in the Gq class: expression in murine tissues and in stromal and hematopoietic cell lines. Proc. Natl. Acad. Sci. U.S.A. **88**: 10049–10053.

Wilkie T. M., Gilbert D. J., Olsen A. S., Chen X. N., Amatruda T. T. *et al.*, 1992 Evolution of the mammalian G protein alpha subunit multigene family. Nat. Genet. **1**: 85–91.

Williams S. L., Lutz S., Charlie N. K., Vettel C., Ailion M. *et al.*, 2007 Trio's Rho-specific GEF domain is the missing Galpha q effector in C. elegans. Genes Dev **21**: 2731–2746.

Xie L., Gao S., Alcaire S. M., Aoyagi K., Wang Y. *et al.*, 2013 NLF-1 delivers a sodium leak channel to regulate neuronal excitability and modulate rhythmic locomotion. Neuron **77**: 1069–1082.

Yeh E., Ng S., Zhang M., Bouhours M., Wang Y. *et al.*, 2008 A putative cation channel, NCA-1, and a novel protein, UNC-80, transmit neuronal activity in C. elegans. PLoS Biol. **6**: e55.

Figure 1

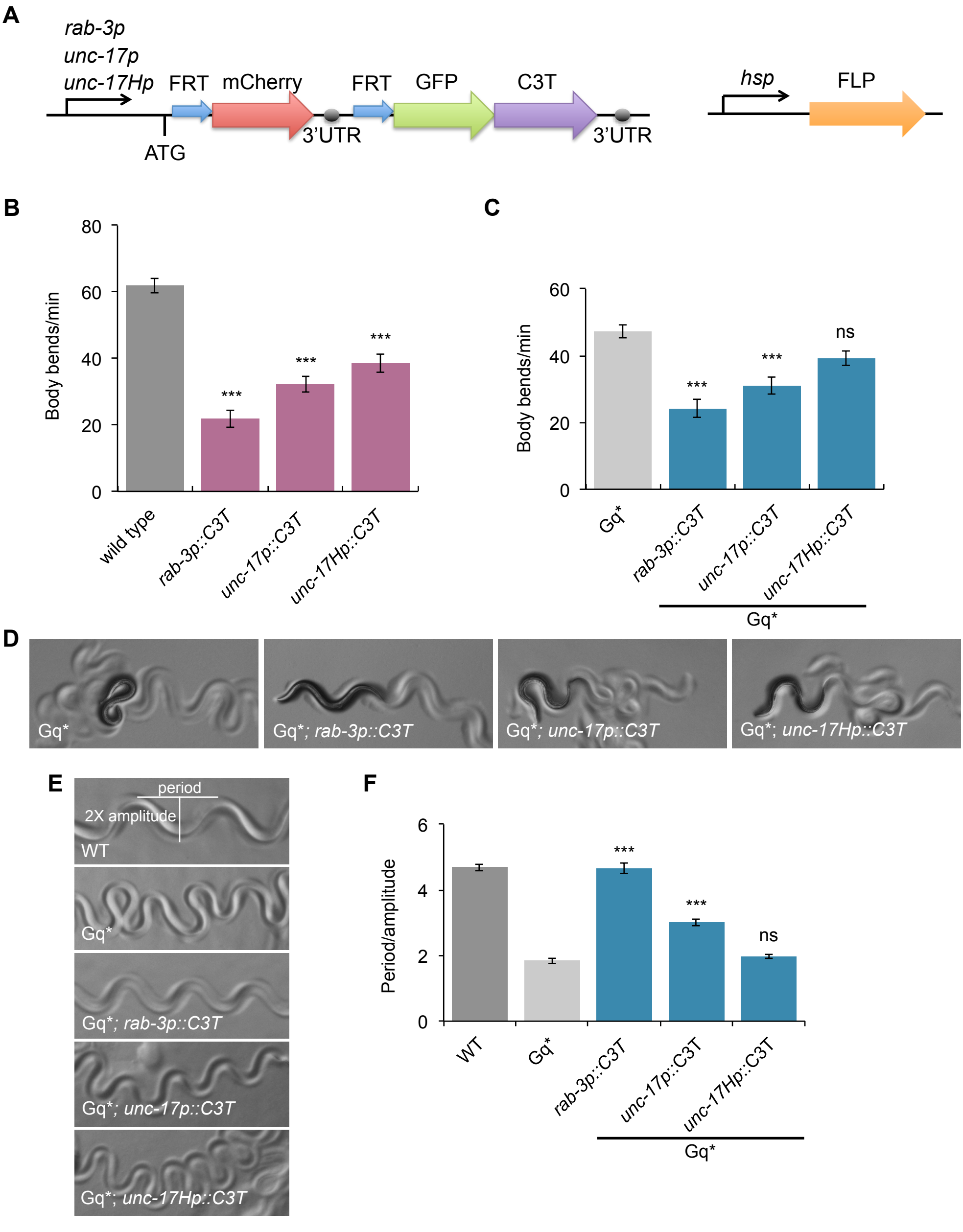
A
rab-3p
unc-17p
unc-17Hp
FRT
mCherry
3'UTR
FRT
GFP
C3T
3'UTR
ATG
hsp
FLP
B
Body bends/min
80
60
40
20
0
***
***
***
wild type
rab-3p::C3T
unc-17p::C3T
unc-17Hp::C3T
C
Body bends/min
60
40
20
0
***
***
ns
Gq*
rab-3p::C3T
unc-17p::C3T
unc-17Hp::C3T
Gq*
D
Gq*
Gq*; rab-3p::C3T
Gq*; unc-17p::C3T
Gq*; unc-17Hp::C3T
E
period
2X amplitude
WT
Gq*
Gq*; rab-3p::C3T
Gq*; unc-17p::C3T
Gq*; unc-17Hp::C3T
F
Period/amplitude
6
4
2
0
***
***
ns
WT
Gq*
rab-3p::C3T
unc-17p::C3T
unc-17Hp::C3T
Gq*

Figure 2

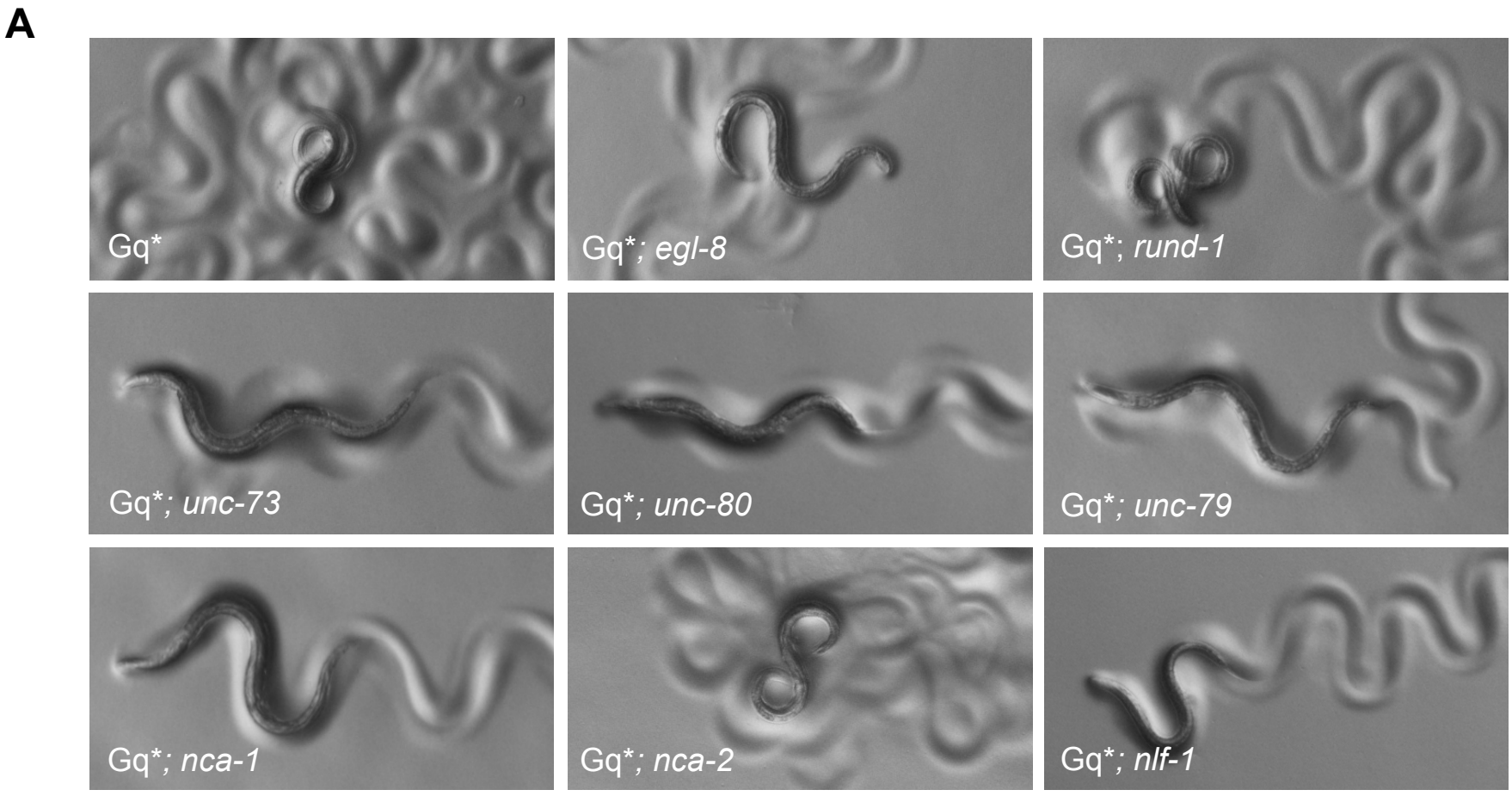
A
Gq*
Gq*; egl-8
Gq*; rund-1
Gq*; unc-73
Gq*; unc-80
Gq*; unc-79
Gq*; nca-1
Gq*; nca-2
Gq*; nlf-1

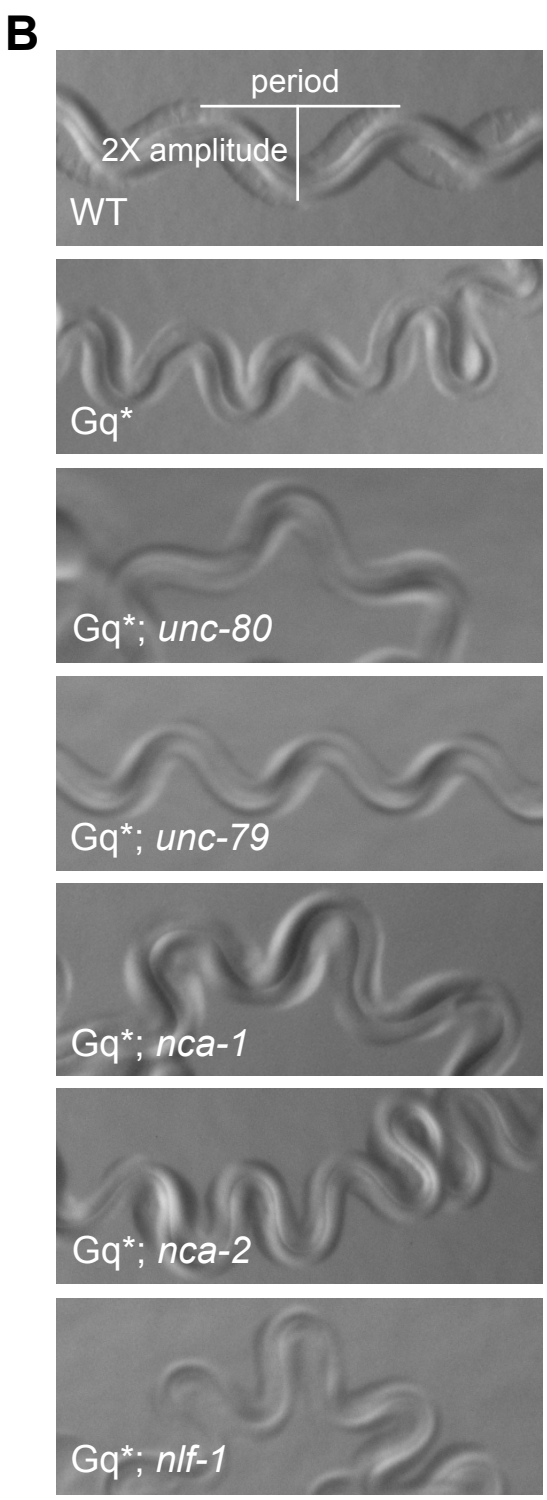
B
period
2X amplitude
WT
Gq*
Gq*; unc-80
Gq*; unc-79
Gq*; nca-1
Gq*; nca-2
Gq*; nlf-1

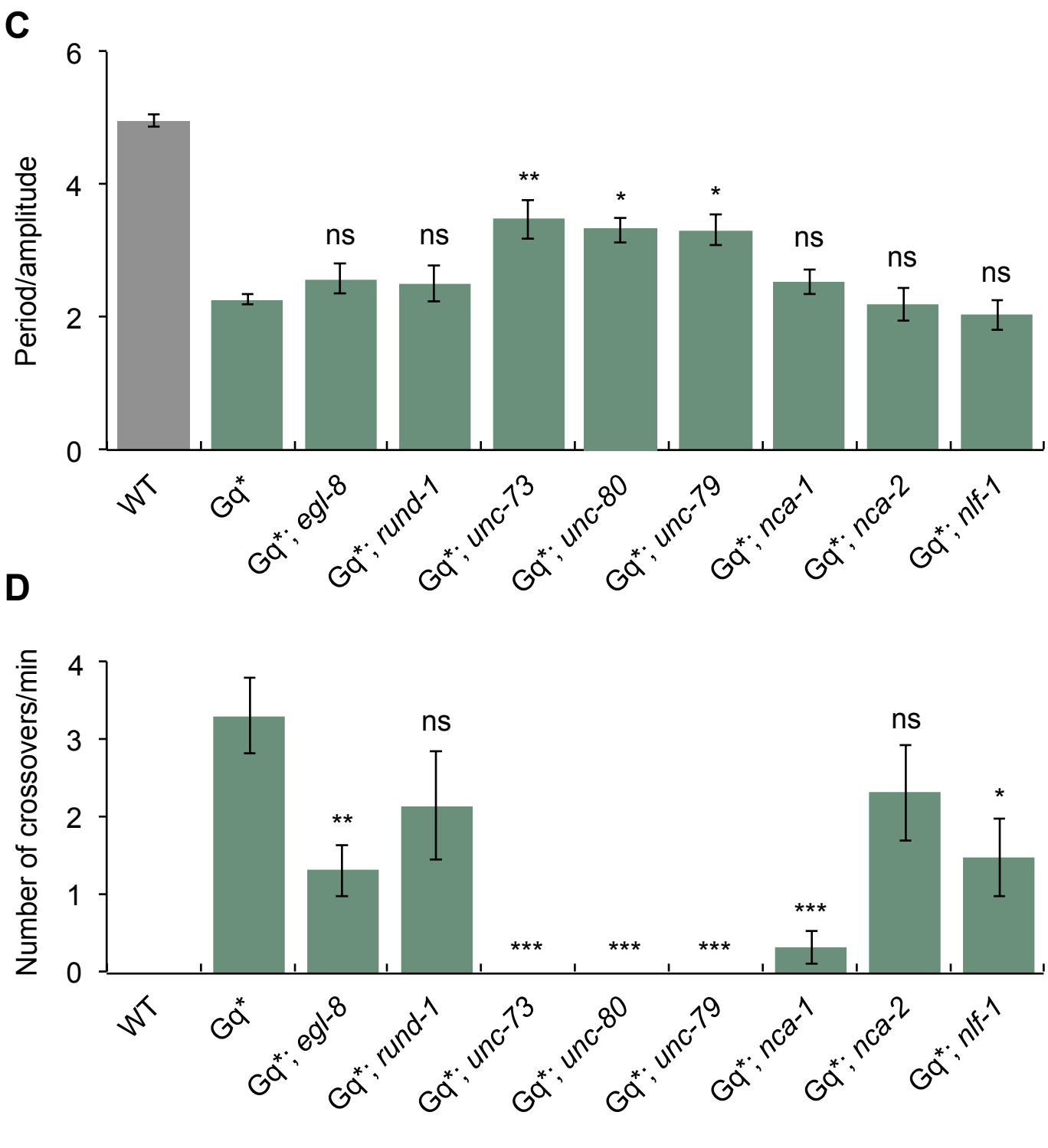
C
Period/amplitude
6
4
2
0
ns
ns
**
*
*
ns
ns
ns
WT
Gq*
Gq*; egl-8
Gq*; rund-1
Gq*; unc-73
Gq*; unc-80
Gq*; unc-79
Gq*; nca-1
Gq*; nca-2
Gq*; nlf-1
D
Number of crossovers/min
4
3
2
1
0
**
ns
***
***
***
***
ns
*
WT
Gq*
Gq*; egl-8
Gq*; rund-1
Gq*; unc-73
Gq*; unc-80
Gq*; unc-79
Gq*; nca-1
Gq*; nca-2
Gq*; nlf-1

Figure 3

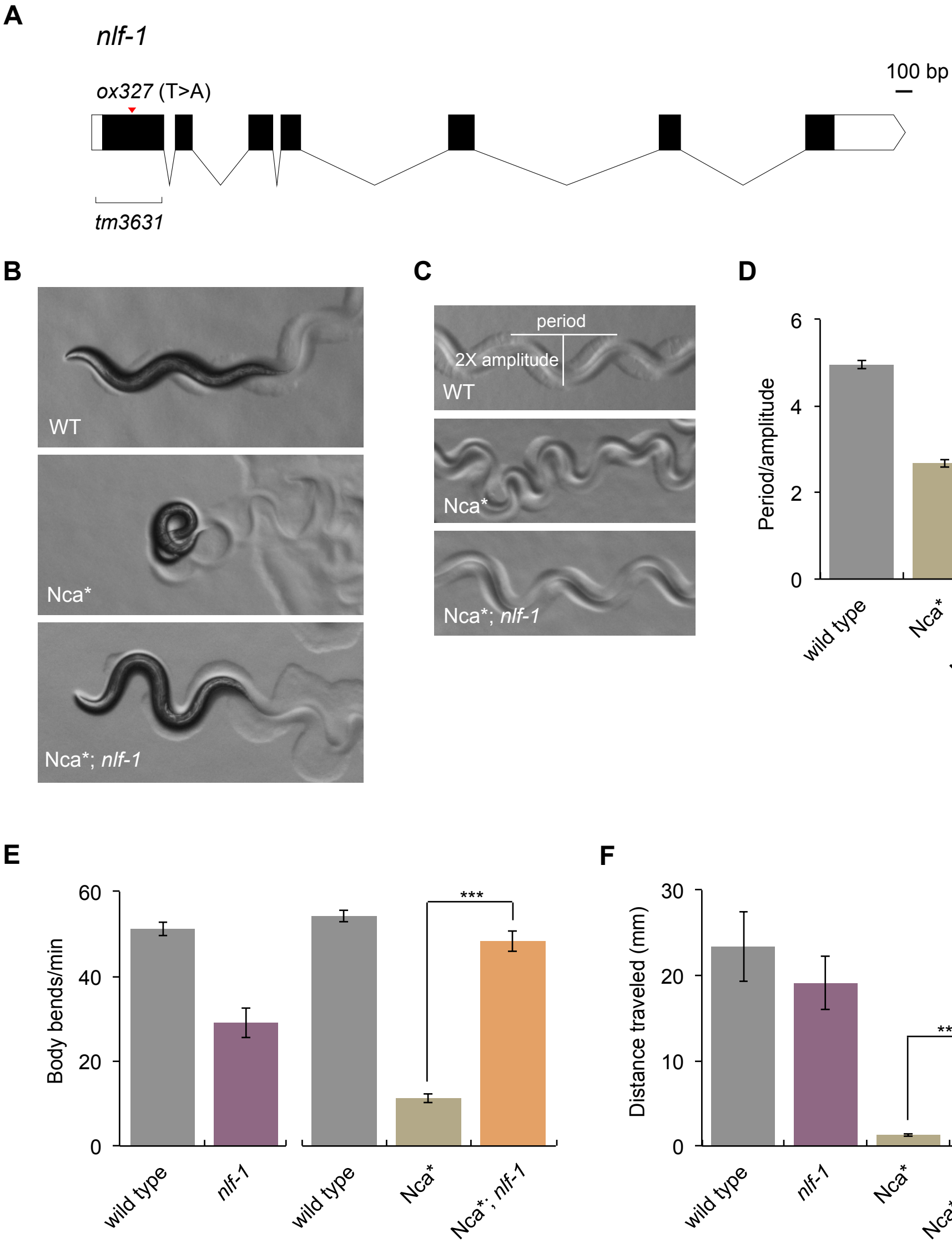
A
nlf-1
ox327 (T>A)
100 bp
tm3631
B
WT
Nca*
Nca*; nlf-1
C
period
2X amplitude
WT
Nca*
Nca*; nlf-1
D
Period/amplitude
6
4
2
0
***
wild type
Nca*
Nca*; nlf-1
E
Body bends/min
60
40
20
0
***
wild type
nlf-1
wild type
Nca*
Nca*; nlf-1
F
Distance traveled (mm)
30
20
10
0
***
wild type
nlf-1
Nca*
Nca*; nlf-1

Figure 4

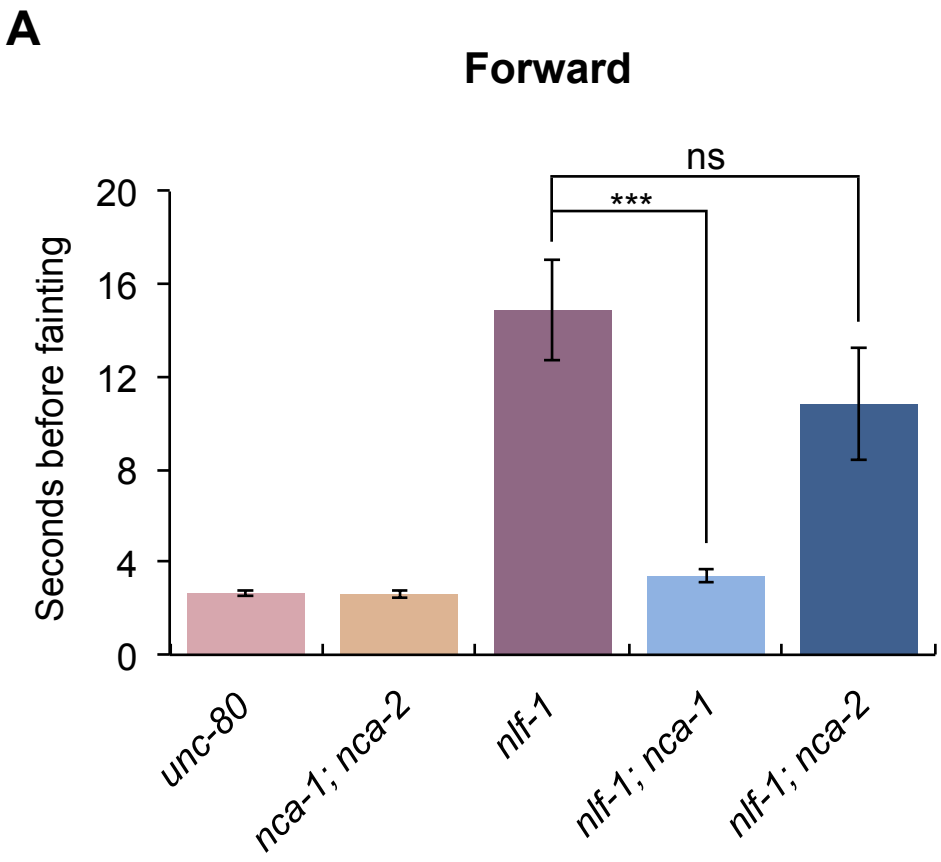
A
Forward
Seconds before fainting
0
4
8
12
16
20
ns
***
unc-80
nca-1; nca-2
nlf-1
nlf-1; nca-1
nlf-1; nca-2

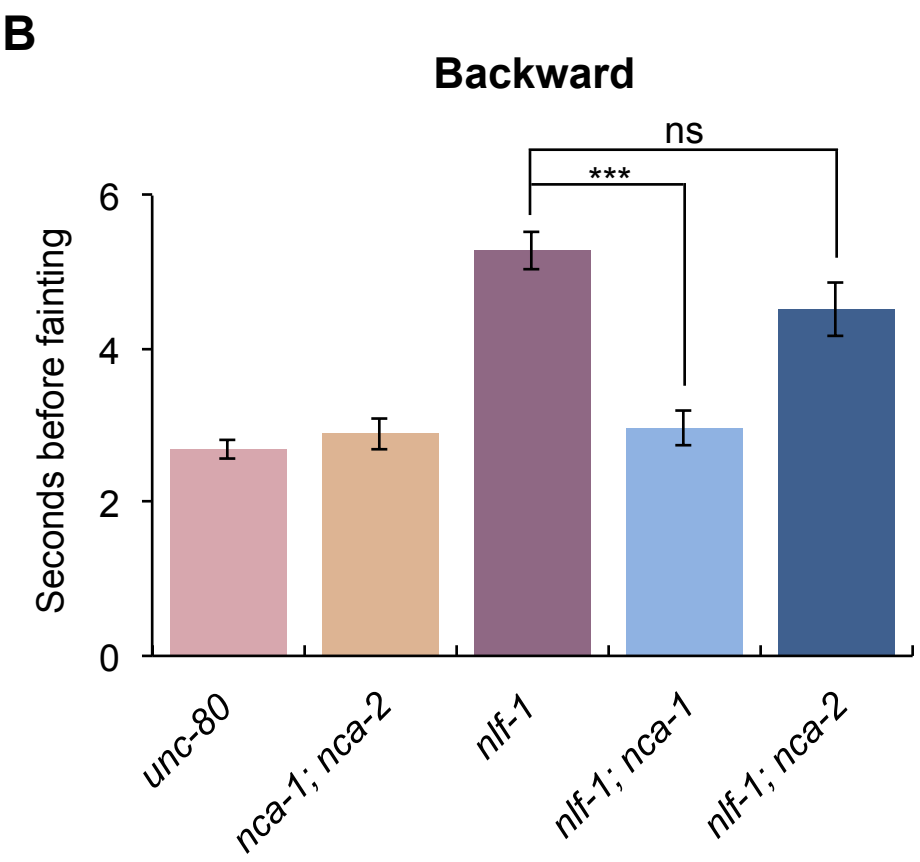
B
Backward
Seconds before fainting
0
2
4
6
ns
***
unc-80
nca-1; nca-2
nlf-1
nlf-1; nca-1
nlf-1; nca-2

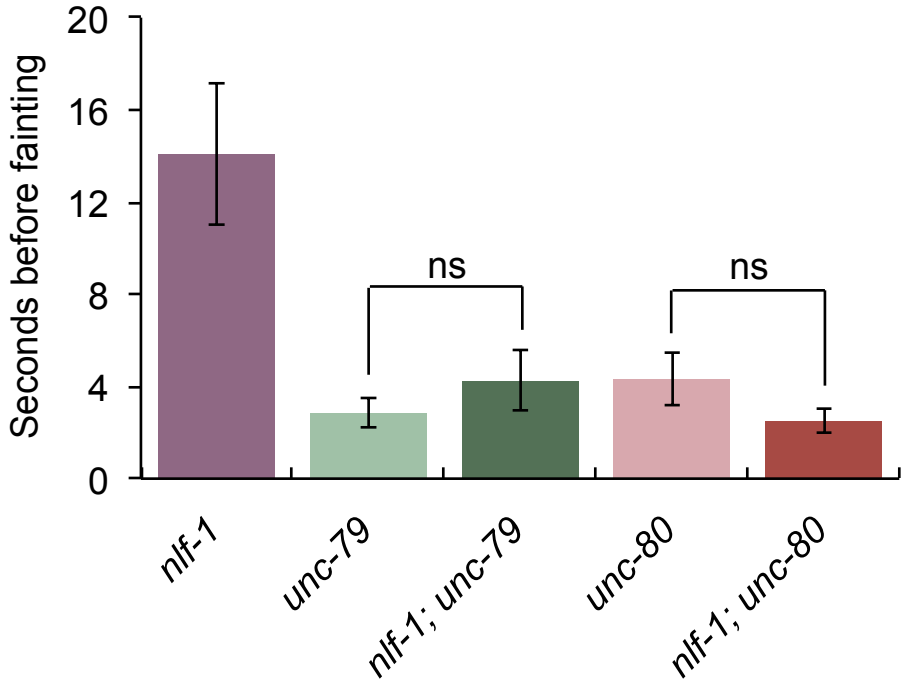
C
Forward
Seconds before fainting
0
4
8
12
16
20
ns
ns
nlf-1
unc-79
nlf-1; unc-79
unc-80
nlf-1; unc-80

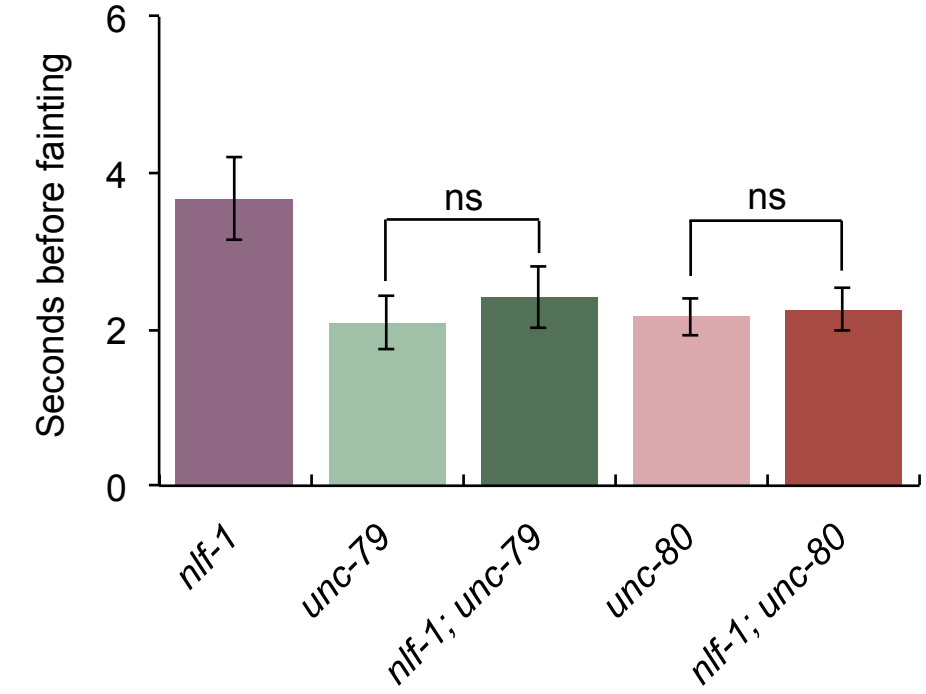
D
Backward
Seconds before fainting
0
2
4
6
ns
ns
nlf-1
unc-79
nlf-1; unc-79
unc-80
nlf-1; unc-80

Figure 5

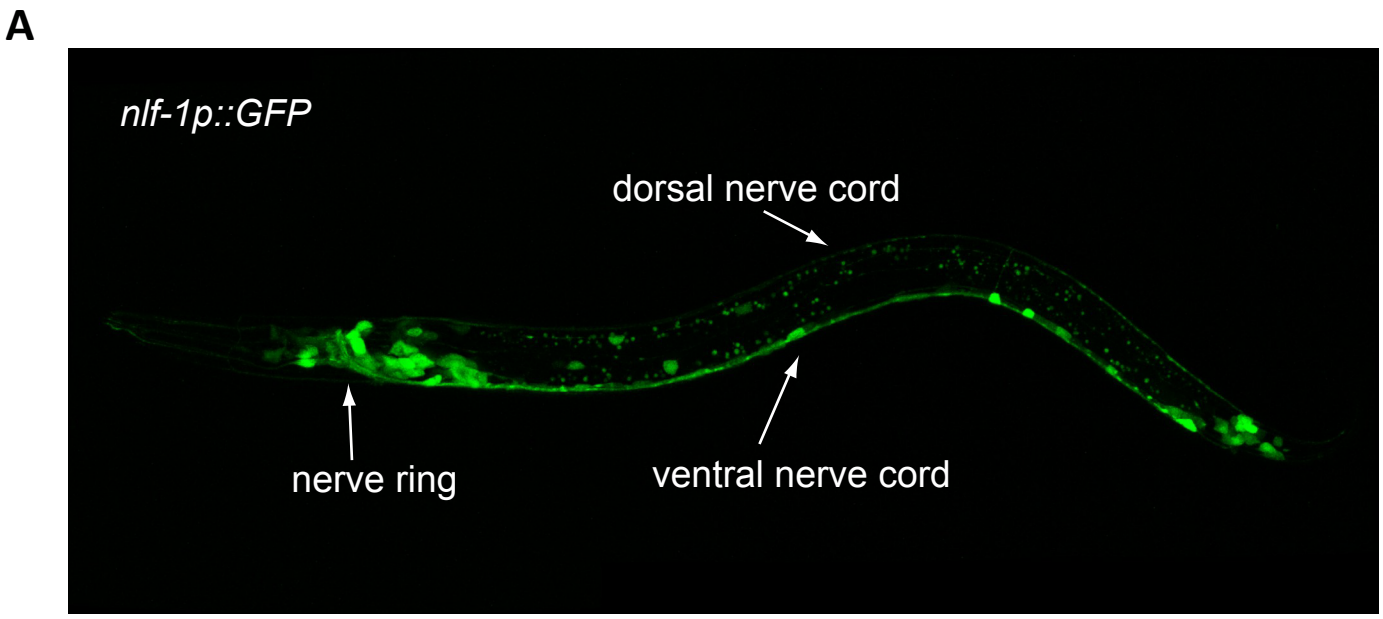
A
nlf-1p::GFP
dorsal nerve cord
nerve ring
ventral nerve cord

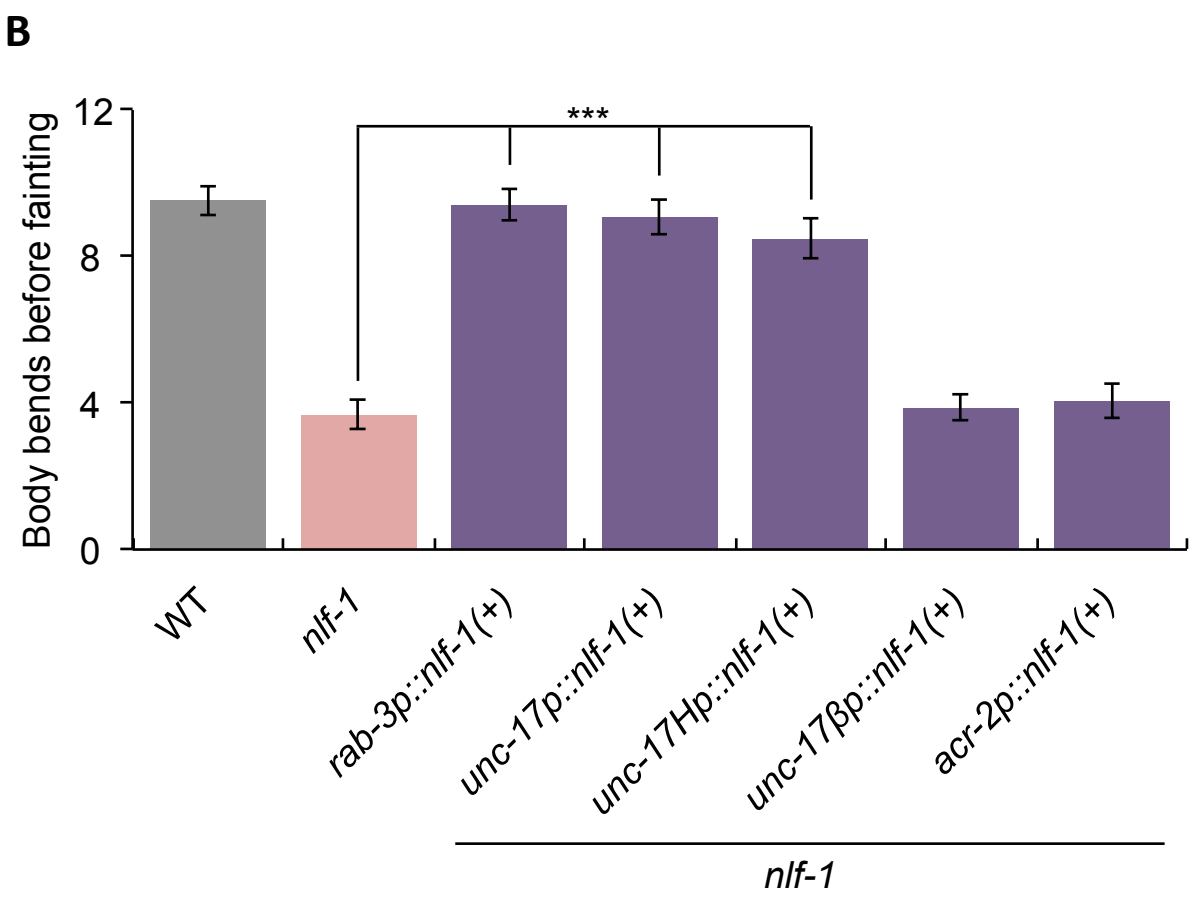
B
Body bends before fainting
12
8
4
0
***
WT
nlf-1
rab-3p::nlf-1(+)
unc-17p::nlf-1(+)
unc-17Hp::nlf-1(+)
unc-17βp::nlf-1(+)
acr-2p::nlf-1(+)
nlf-1

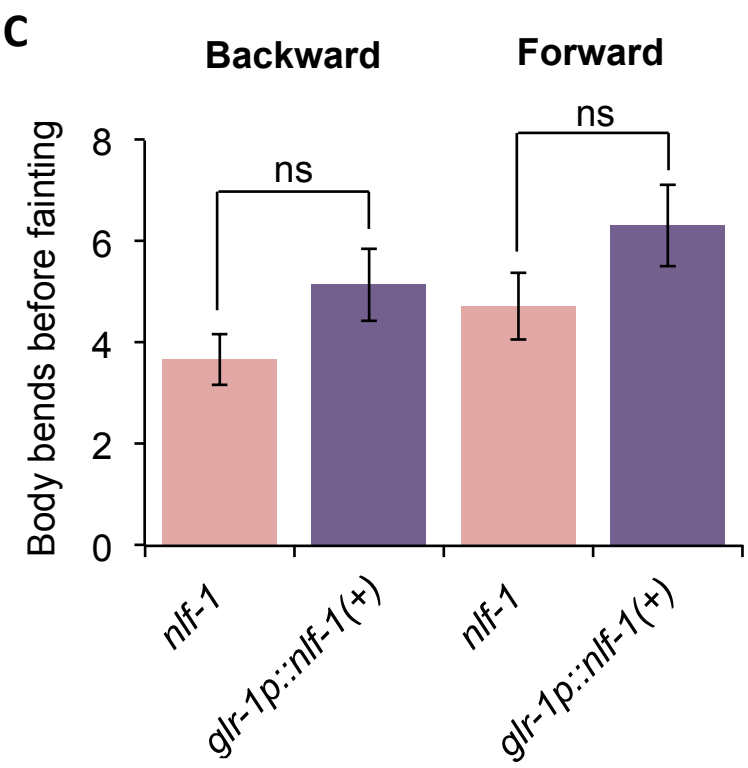
C
Backward
Forward
Body bends before fainting
8
6
4
2
0
ns
ns
nlf-1
glr-1p::nlf-1(+)
nlf-1
glr-1p::nlf-1(+)

Figure 6

A

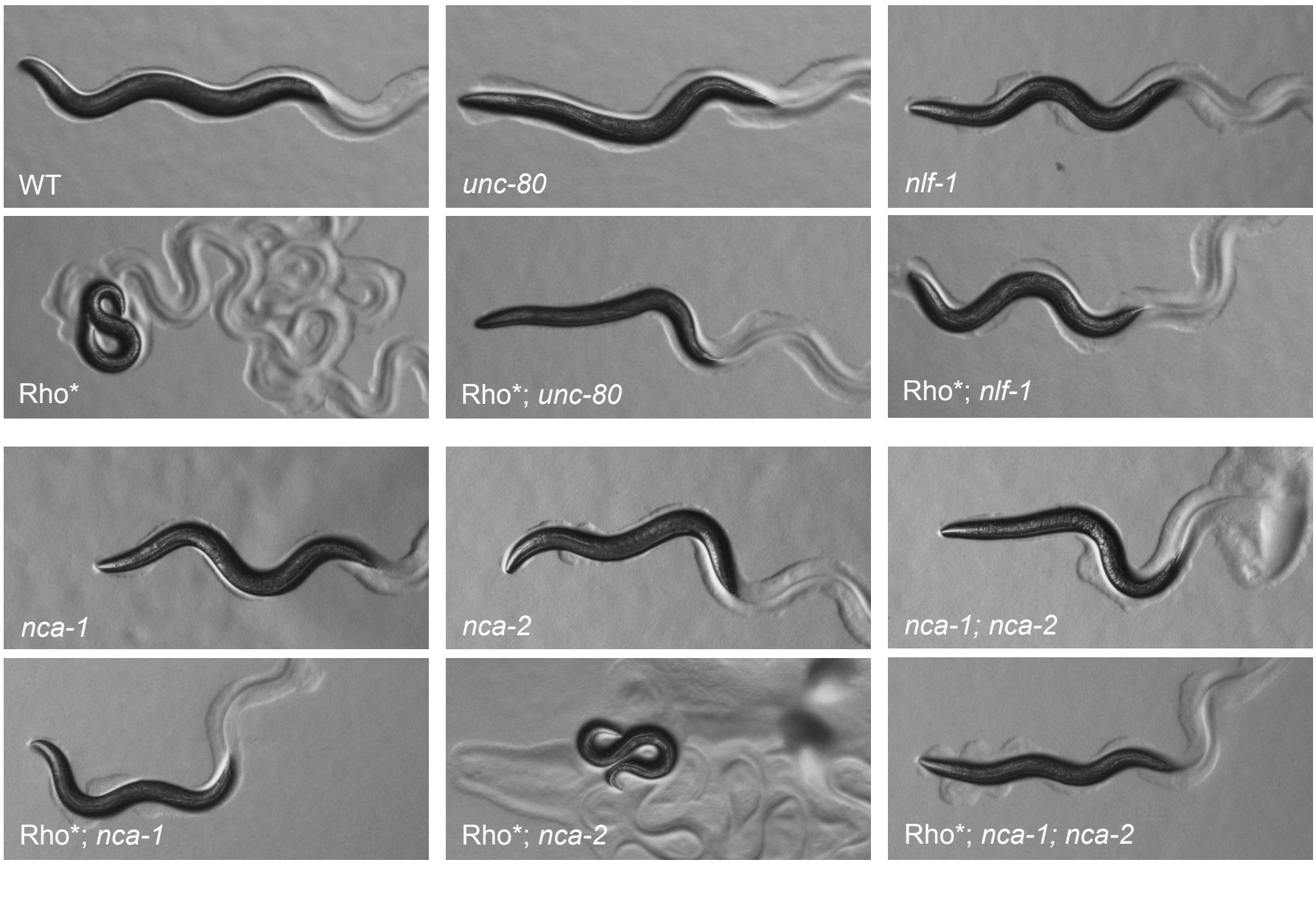
WT
unc-80
nlf-1
Rho*
Rho*; unc-80
Rho*; nlf-1
nca-1
nca-2
nca-1; nca-2
Rho*; nca-1
Rho*; nca-2
Rho*; nca-1; nca-2

B

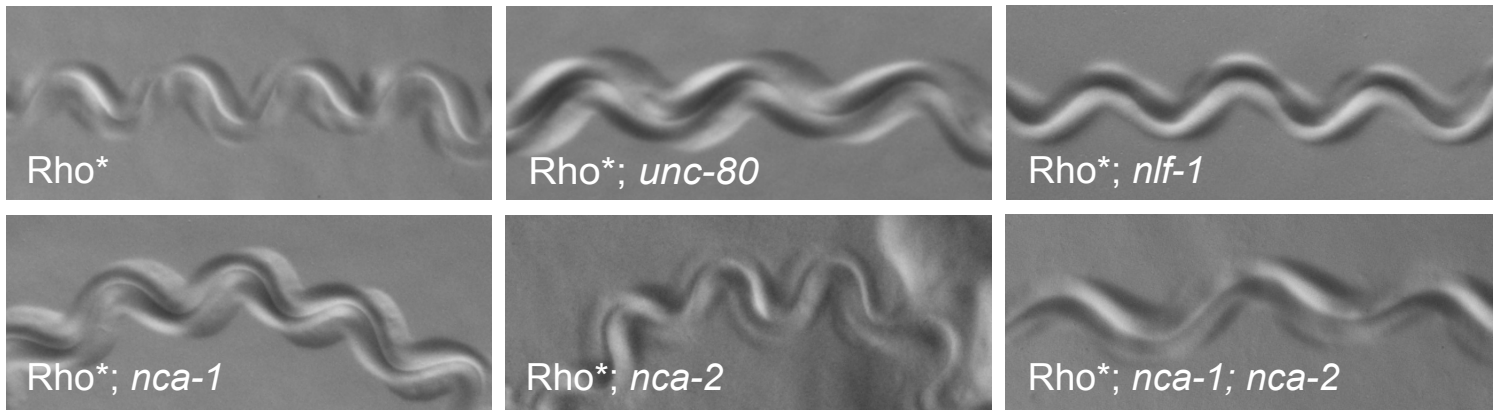
Rho*
Rho*; unc-80
Rho*; nlf-1
Rho*; nca-1
Rho*; nca-2
Rho*; nca-1; nca-2

C

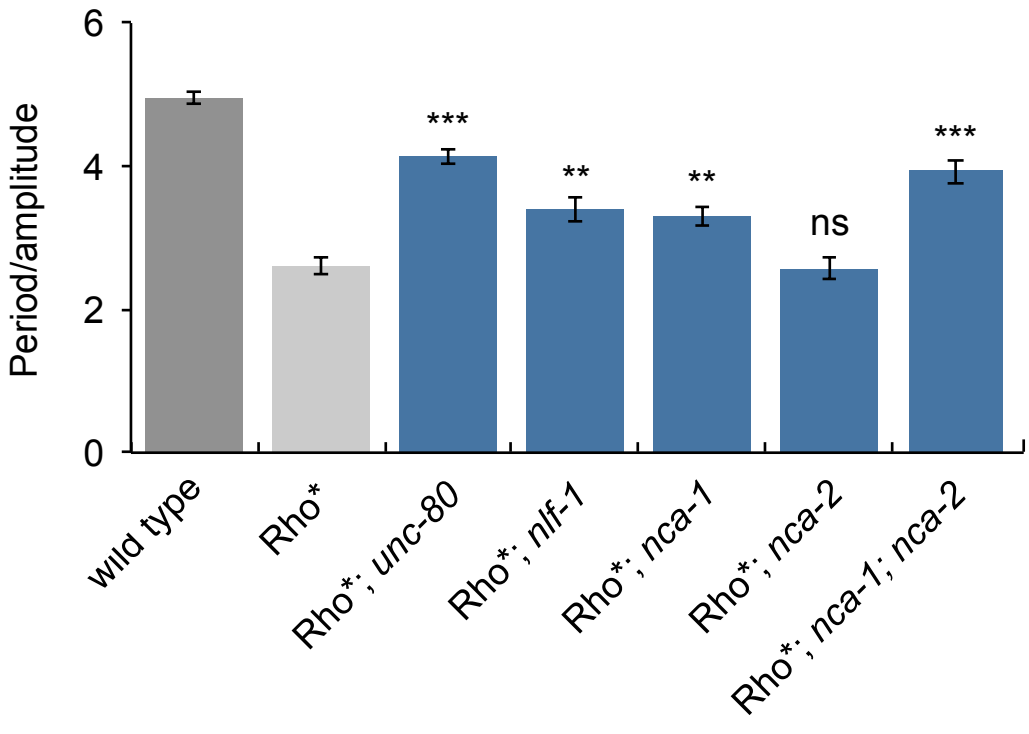
Period/amplitude
6
4
2
0
***
**
**
ns
***
wild type
Rho*
Rho*; unc-80
Rho*; nlf-1
Rho*; nca-1
Rho*; nca-2
Rho*; nca-1; nca-2

Figure 7

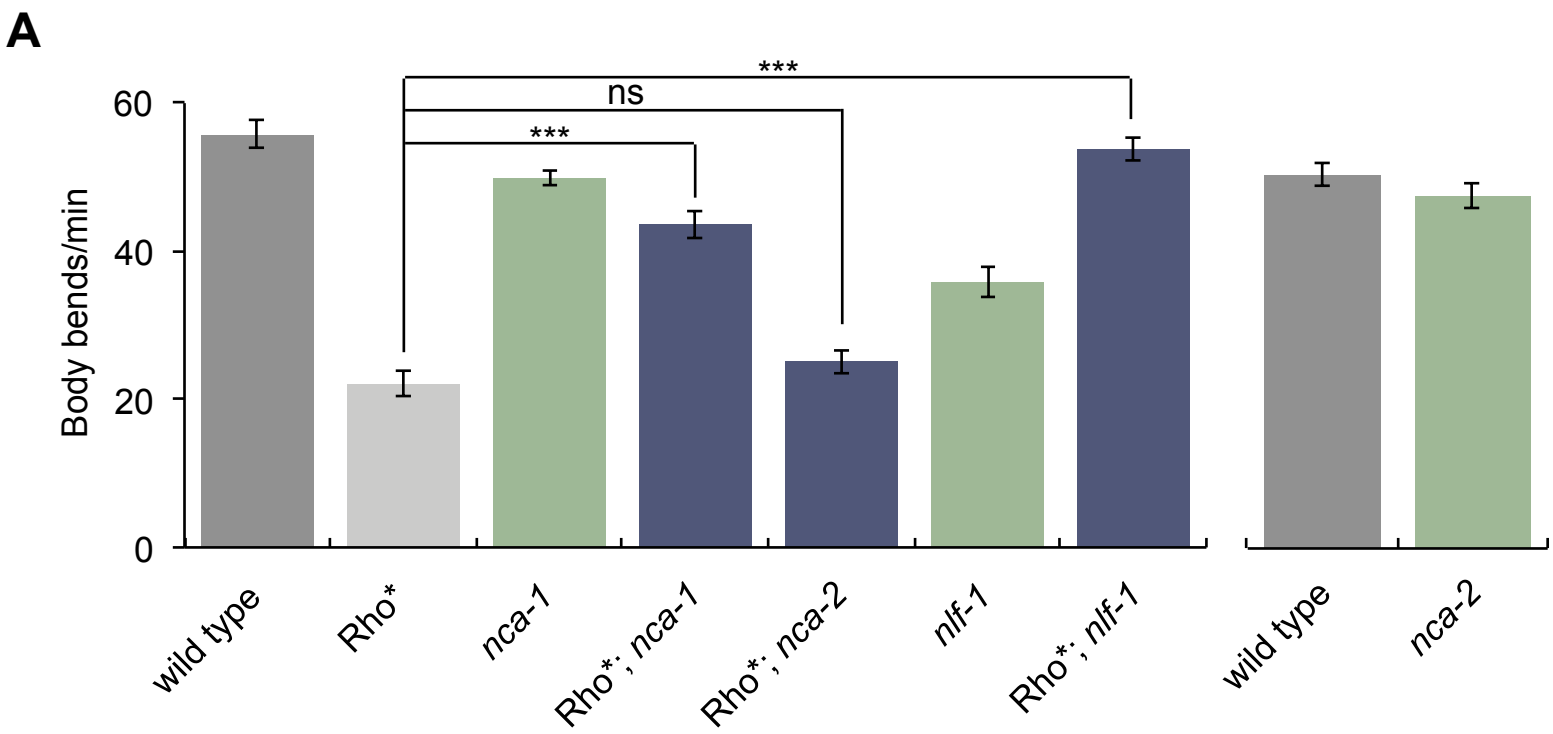
A
Body bends/min
60
40
20
0
***
ns
***
wild type
Rho*
nca-1
Rho*; nca-1
Rho*; nca-2
nlf-1
Rho*; nlf-1
wild type
nca-2

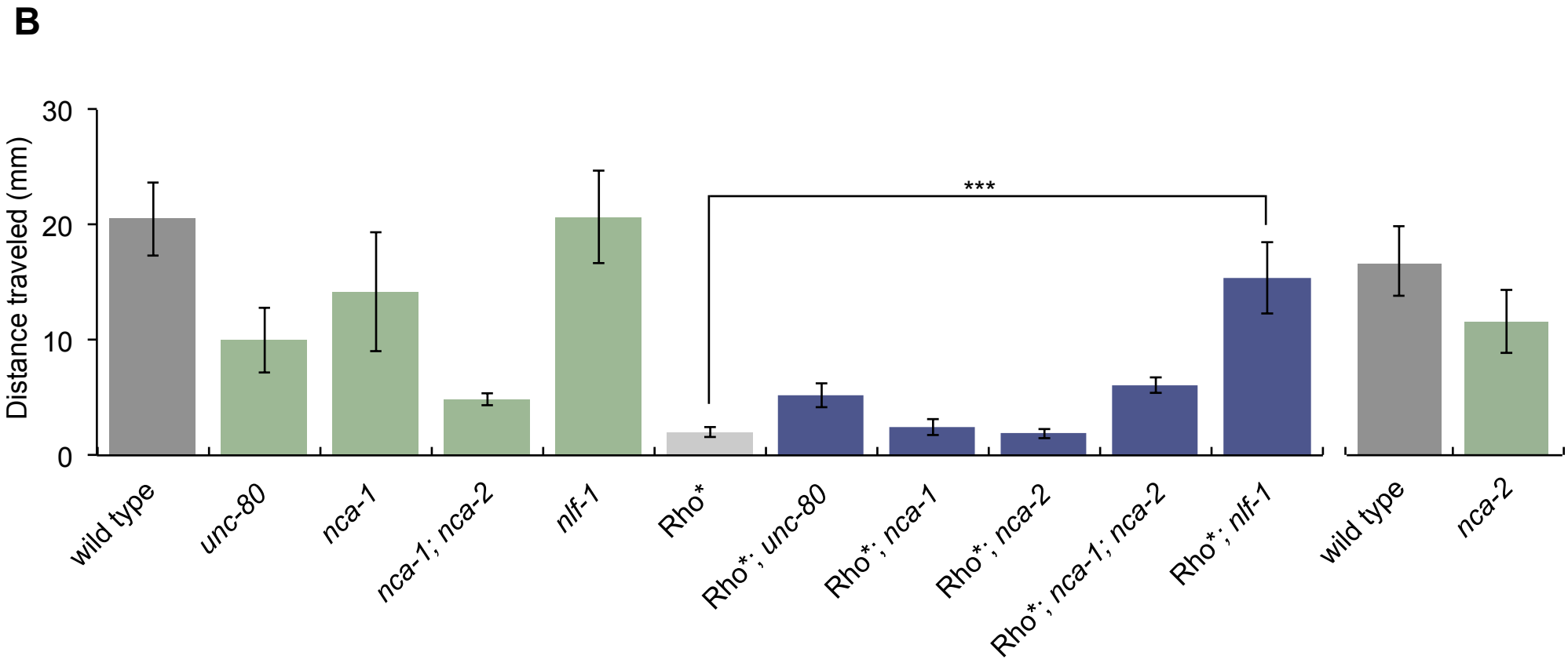
B
Distance traveled (mm)
30
20
10
0
***
wild type
unc-80
nca-1
nca-1; nca-2
nlf-1
Rho*
Rho*; unc-80
Rho*; nca-1
Rho*; nca-2
Rho*; nca-1; nca-2
Rho*; nlf-1
wild type
nca-2

Figure 8

A

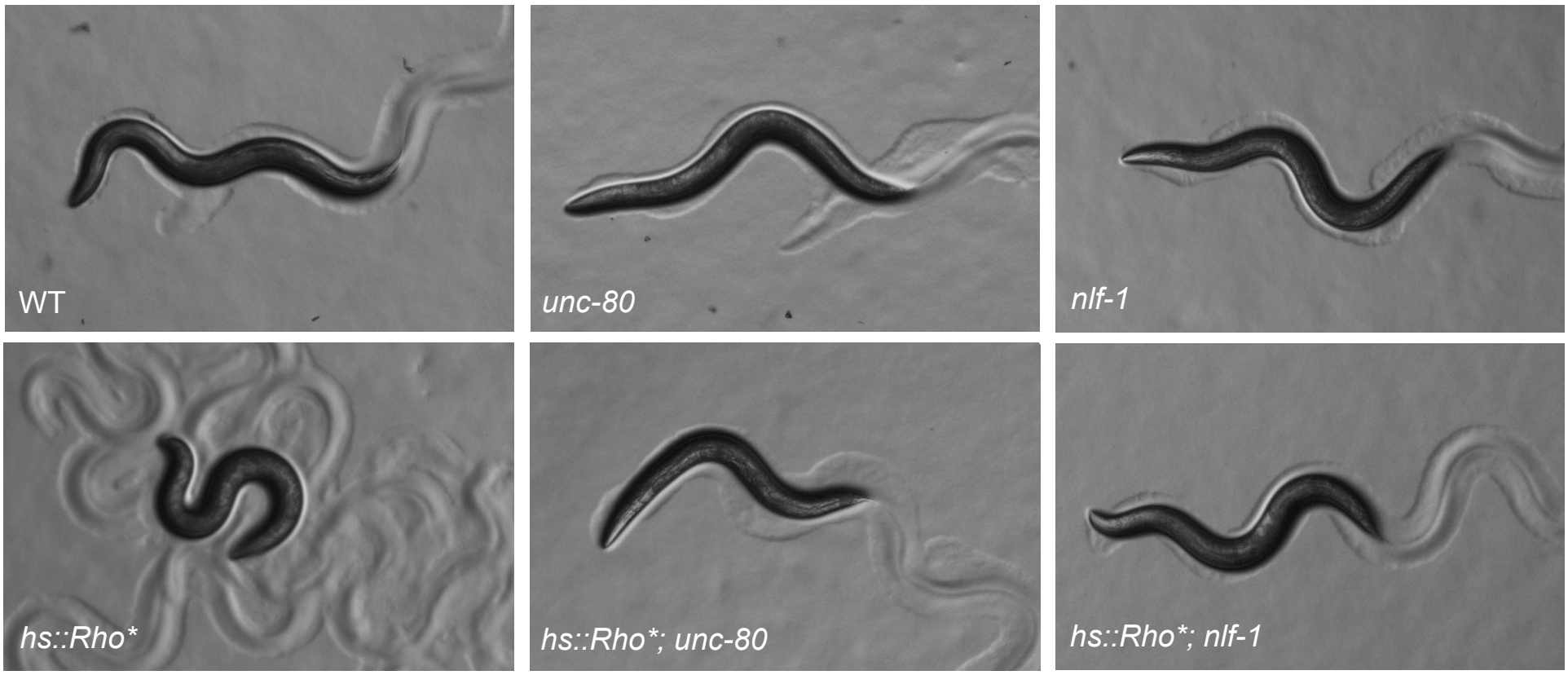

B

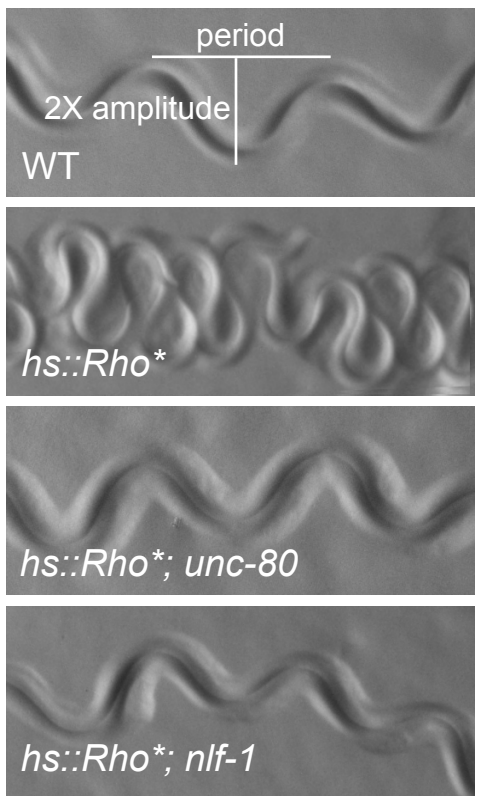

C

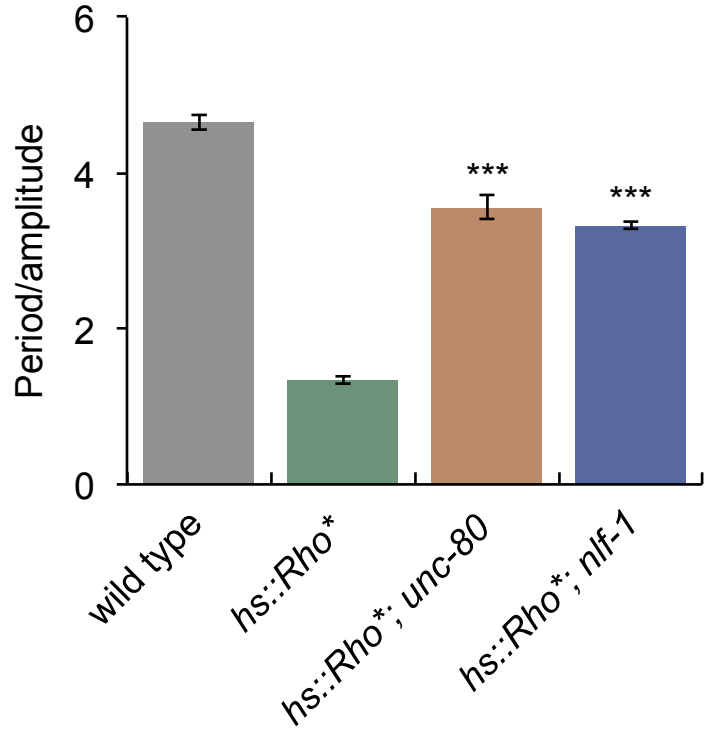

D

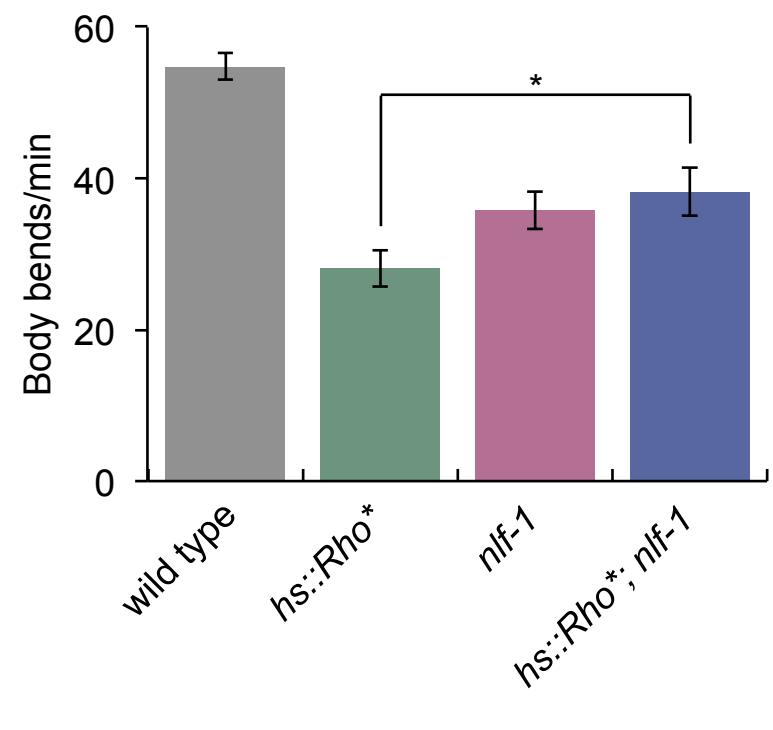

Figure 9

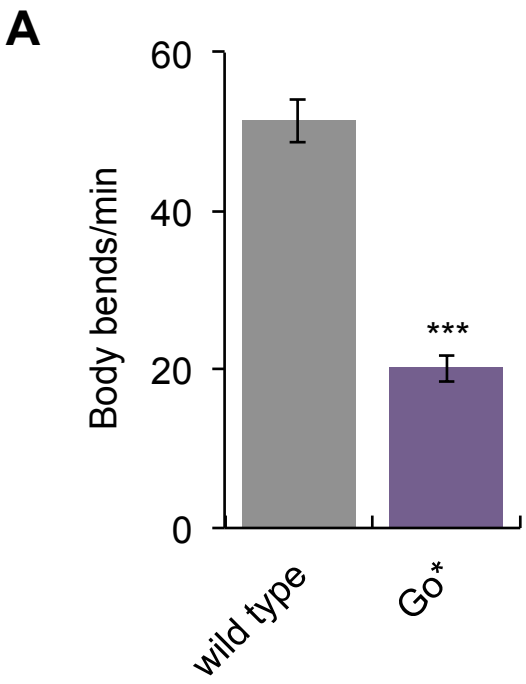
A
60
40
20
0
Body bends/min
***
wild type
Go*

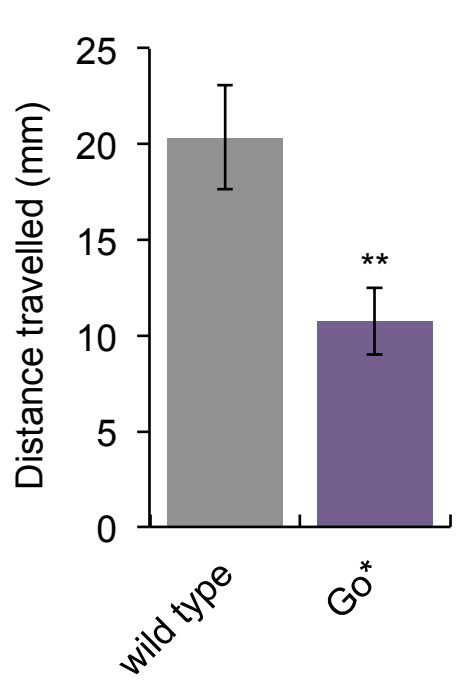
B
25
20
15
10
5
0
Distance travelled (mm)
**
wild type
Go*

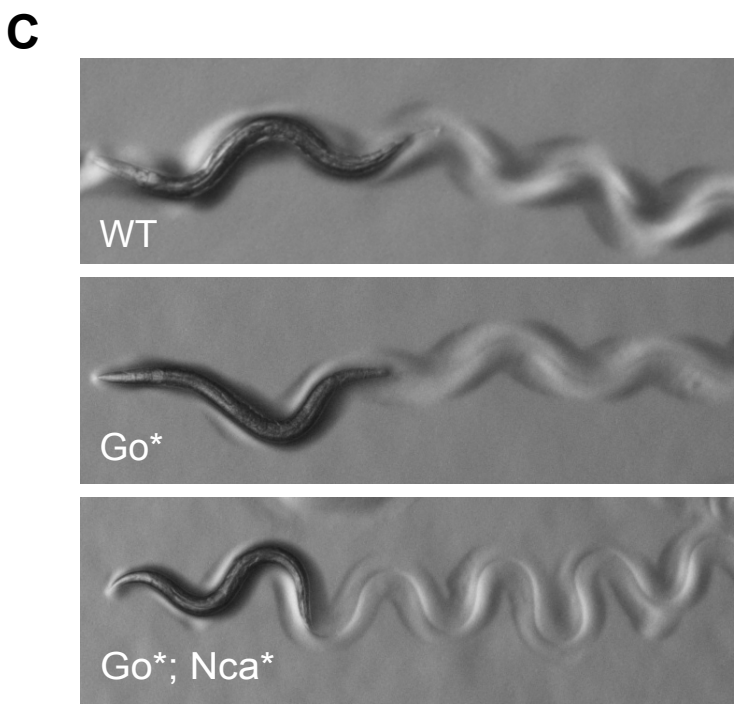
C
WT
Go*
Go*; Nca*

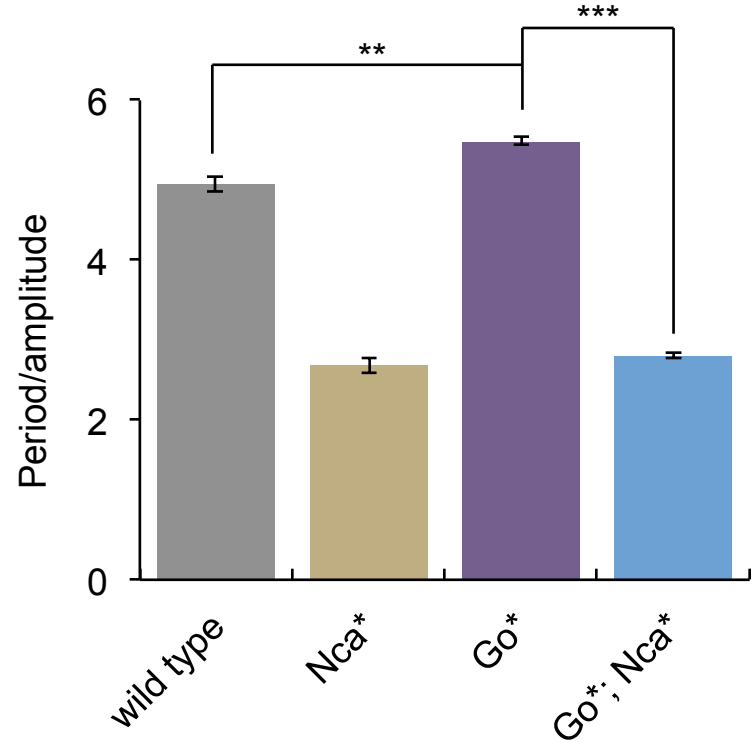
D
**
***
6
4
2
0
Period/amplitude
wild type
Nca*
Go*
Go*; Nca*

Figure 10

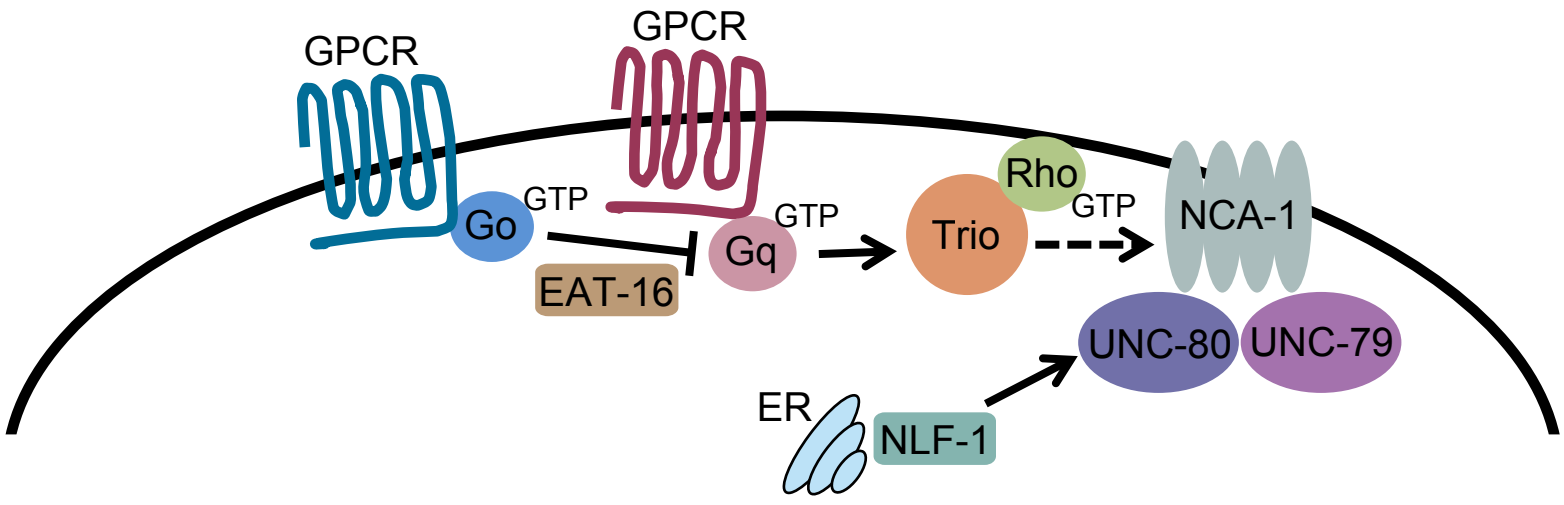
GPCR
GPCR
Go
GTP
EAT-16
Gq
GTP
Trio
Rho
GTP
NCA-1
UNC-80
UNC-79
ER
NLF-1